

STRANGENESS CONSERVATION IN HOT FIREBALLS

Jean Letessier

Ahmed Tounsi

Laboratoire de Physique Théorique et Hautes Energies, Paris*

Ulrich Heinz

Josef Sollfrank

Institut für Theoretische Physik, Universität Regensburg†

and

Johann Rafelski

Department of Physics, University of Arizona, Tucson, AZ 85721

Abstract

A constraint between thermal fireball parameters arises from the requirement that the balance of strangeness in a fireball is (nearly) zero. We study the impact of this constraint on (multi-)strange (anti-)baryon multiplicities and compare the hadron gas and quark-gluon plasma predictions. We explore the relation between the entropy content and particle multiplicities and show that the data are compatible with the quark-gluon plasma hypothesis, but appear to be inconsistent with the picture of an equilibrated hadron gas fireball. We consider the implications of the results on the dynamics of evolution and decay of the particle source.

Submitted to Physical Review D

PAR/LPTHE/92-27

TPR-92-28

AZPH-TH/92-23

November 1992

*Unité associée au CNRS, Université PARIS 7, Tour 24, 5è ét., 2 Place Jussieu, F-75251 CEDEX 05, France.

†Institut für Theoretische Physik, Universität Regensburg, Postfach 10 10 42, W-8400 Regensburg, Germany

1 Introduction

The reported enhancement of strange particle production in heavy ion collisions relative to proton-proton and proton-nucleus collisions [1] tells us that we are dealing with a state of matter which is *i)* very dense or *ii)* relatively long-lived, or in which *iii)* strangeness production cross sections are enhanced, or which *iv)* possesses some combination of these three factors. In order to be able to be more specific about the nature of the dense matter, the relative production abundances of strange and multi-strange baryons and anti-baryons were studied. They turned out to be particularly sensitive probes of the thermal conditions of their source [2, 3]. Studies of the properties of a hadron resonance gas fireball including strange particles have shown [4, 5, 6, 7] that the constraint of vanishing net strangeness of the emitting source leads to similar thermal and chemical conditions for both a hadronic gas (HG) and a deconfined quark-gluon plasma (QGP) fireball, if the temperature is taken to be near $T = 210 \pm 10$ MeV. This value was extracted [8] from the m_{\perp} -spectra from 200 GeV A S–W and S–Pb collisions under the assumption that their slope is dominated by the thermal motion of the particles at freeze-out and does not contain a collective flow component [9]. We will discuss that the observed smallness of the strange quark chemical potential appears to be inconsistent with the presence of a strong flow component in the spectra.

It has already been pointed out [6] that near $T = 210$ MeV further information, such as the particle multiplicity per participant nucleon, may help to distinguish QGP from the HG. Following this route, we will show here in detail [10] that the data of emulsion experiment EMU05 [11] indeed appear to be incompatible on these grounds with the hadronic gas fireball model. Further support for a new physical state such as the quark-gluon plasma as the source of these anti-baryons may be obtained by studying the response of the measured parameters to changes in beam energy or size of the colliding nuclei. Our work has been in part motivated by the imminent extension of the experimental program at CERN and BNL to heavy nuclear projectiles (Pb and Au, respectively), and by the prospect of higher (and lower) beam energies becoming available, in particular towards the end of the decade at Brookhaven with RHIC and possibly at CERN with LHC. Therefore, in addition to $T \simeq 200$ MeV appropriate for the CERN–SPS energy range, we also include in our discussion the parameter range ($T \simeq 150$ MeV) suitable for the current BNL heavy-ion experiments at 10–15 GeV A and for potential future low beam energy runs at CERN, as well as $T \simeq 300$ MeV, which we judge appropriate for the future RHIC and LHC facilities [12].

Our expectation is that, as the conditions of the experiments are changed, we will be able to study the response of the statistical parameters such as the strange quark chemical potential μ_s or the strangeness saturation factor γ_s . These parameters show characteristic differences in a hadron gas and a QGP: γ_s , for example, is expected to rapidly approach unity for increasing four-volume of the QGP fireball, while remaining small in HG fireballs [13]. The strange quark chemical potential μ_s , on the other hand, has the characteristic property that it is exactly zero in a strangeness-zero QGP fireball, independent of its baryon density. In contrast to this, μ_s is generally different from zero in conventional hadronic gas reactions, except for the special case of baryon-free matter with $\mu_B = 0$; however, if T is not too large ($T < 220$ MeV), for each value of the temperature a certain value of baryochemical potential $\mu_B \neq 0$ can be found for which also $\mu_s^{\text{HG}} = 0$. This value generally depends on the detailed form of the equation of state (EoS), and for the case of a conventional (Hagedorn type) HG

it has been discussed in Refs. [6, 14]. While the large values of γ_s which are characteristic of the fast chemical kinetics in a QGP are largely preserved during hadronization, the value of μ_s is usually subject to modifications, in particular if the phase transformation occurs slowly. Experimentally, the values of μ_s and γ_s are reflected in the observed strange hadron ratios (where, as we will discuss, in the case of QGP certain model assumptions for the hadronization process are necessary in order to quantify this relationship), which allows for a rather straightforward experimental test of the fireball picture, of the concept of (absolute or relative) chemical equilibrium, and of the nature (HG or QGP) of the collision fireball.

In order to distinguish between the two phases by studying particle production as the conditions of the experiments are changed we need to understand also in the HG phase how the strange chemical potential μ_s relates to the baryochemical potential μ_B in the collision fireball. Such a relationship is required by the fact that the total strangeness in the initial state is zero, and that strangeness is conserved by strong interactions. Thus, up to (presumably small) pre-equilibrium emission effects which can introduce a small strangeness asymmetry $\bar{s} - s \equiv \varepsilon s$, the number of strange and anti-strange quarks in the fireball are equal ($\varepsilon \simeq 0$). We work out in detail how the strange chemical potential is determined at fixed temperature by the baryochemical potential and a given (small) fraction ε of net strangeness in the fireball. We find that at a fireball temperature around $T = 210$ MeV, there is a peculiar behavior of μ_s which causes a particular insensitivity of the strange anti-baryon ratios alone to the structure of the source. In order to be able to reach a conclusion about the internal structure of the source, we then study the entropy content of the particle source. We also show that the kaon to hyperon ratio is a poor signature for the nature of the source, but could be a good measure of the baryochemical potential [15].

The HG part of our work is similar in spirit, but different in detail from the parallel effort of Cleymans and Satz [7]¹. We study particle ratios at fixed transverse mass $m_\perp > 1.7$ GeV. We allow for the strangeness phase space to be only partially saturated and show how the degree of saturation γ_s can be experimentally measured in order to later serve as a test for the kinetic theory of strangeness production. We allow the strangeness to be slightly unbalanced (up to 10%) and discuss the corresponding variations in the observables. Furthermore we compare the entropy content for the two different scenarios (HG and QGP) and confront the findings with the observed particle multiplicity. In particular we consider the ratio of net charge to total charged multiplicity, $D_Q \equiv (N^+ - N^-)/(N^+ + N^-)$, which can be measured (without identifying particles) with any tracking device within a magnetic field; we show that this ratio is directly related to the specific entropy \mathcal{S}/\mathcal{B} of the fireball, which should be considerably larger for a QGP than for a HG [6]. Since, due to the different stopping, the experimental results from S-S and S-W collisions at 200 GeV A are not in the same class, we avoid combining these results because this would weaken the conclusions from our analysis. We do not combine in our analysis the global kaon data with anti-hyperon data, since low p_\perp kaons, unlike strange anti-baryons, can also arise from peripheral, spectator related processes and other rescattering processes and are therefore not necessarily messengers from the same stages of the collision. Instead we consider the Λ/p and $\bar{\Lambda}/\bar{p}$ as well as Ω/Ξ^- and $\bar{\Omega}/\bar{\Xi}^-$

¹When comparing the present work with Ref. [7], it should be noted that these authors use as the strangeness potential the chemical potential μ_S of the (anti-)hyperon number, while we prefer to work directly with the strange quark chemical potential μ_s . The relationship between their μ_S and our μ_s is given by $\mu_s = \mu_B/3 - \mu_S$.

ratios which, as we will explain, provide independent tests of the degree of strangeness saturation γ_s .

At this point it is worth recording that if a QGP state was formed (as may be indicated by the relatively large value of γ_s , see below), the strangeness pair abundance per participating baryon in this state would be about a factor 2.5 larger compared to hadronic gas interactions. On the other hand, there would be a similar enhancement in the produced entropy (which will manifest itself in the total multiplicity), resulting in a difficulty to identify the absolute enhancement of both quantities: the simplest observable, the K/π ratio, is therefore not a very good discriminator in this context [16]. As we will show, measurement of the specific entropy \mathcal{S}/\mathcal{B} , either globally via the total particle multiplicity per participating nucleon, or (better, see below) in the same kinematic range where the produced strange particles are observed via the ratio $D_Q = (N^+ - N^-)/(N^+ + N^-)$, can remove this ambiguity.

One of the important objectives we pursue is to present a large number of predictions for (strange) particle production which are capable to test the internal consistency of the model developed here and can shed new light on the problem of distinguishing the HG and QGP fireballs. These predictions are quantitative for the S–W collision system at 200 GeV A, but are of a more qualitative nature for the yet unexplored Pb–Pb collisions where we cannot predict precisely the governing statistical parameters (temperature, chemical potentials). We also discuss the systematic behavior of the different statistical model observables in changing environments.

Perhaps the most notable conclusion we reach concerns the model of hadronization of the fireball: we conclude that the only consistent model of the reaction involves explosive disintegration of a QGP as the source of the observed strange anti-baryons. This allows the chemical potentials of the quarks in the QGP phase to get transferred without modification to the observed high- m_\perp strange baryons and anti-baryons, via quark coalescence, and explains naturally the observed vanishing of the strange chemical potential. Since only high m_\perp domain of strange anti-baryon spectra has been experimentally explored, the simple picture of a complete explosion is not absolutely necessary. It is conceivable that at low m_\perp , in particular for low- p_\perp pions, another slower hadronization mechanism also plays a role. We do see the need for some mechanism that produces additional pions, in excess over those obtained from the explosive quark coalescence picture, in order to save the entropy balance and to account for the relatively large observed multiplicity densities. These excess pions (plus perhaps some other light mesons) could easily arise from the gluons in the QGP which carry a large fraction of its entropy. A quantitative formulation of such a hadronization model, however, is not yet available and would require additional data on the detailed origin of the excess multiplicity and its distribution in momentum space.

Naturally, these conclusions rest on the assumed validity of the thermal fireball model. While at present the number of parameters just equals the number of independent observables, the model has considerable predictive power and, with the help of the predictions presented in this paper, its validity will be (hopefully soon) tested. Other pictures for the source of the observed hadrons, such as an equilibrated HG or a QGP fireball which evolves slowly and in full equilibrium into a HG fireball, can not account consistently for certain important experimental features of strange anti-baryon production.

In section 2 we present our thermal model with special attention given to the parameters describing the chemical equilibrium. We take into account the u - d asymmetry and study the

condition of strangeness balance. In section 3 we determine the thermodynamical parameters using the WA85 data on strange baryon and anti-baryon production (with and without taking into account resonance decays). In section 4 the implication of these parameters on the entropy content of the QGP and HG fireballs and on the multiplicity are discussed. We then confront our model with EMU05 and NA35 data. In section 5 we discuss the implications of our results regarding the nature of the initial fireball and the dynamic of its evolution. We give some concluding remarks concerning the distinction we draw between QGP and HG.

2 Thermal models

The use of thermal models to interpret data on particle abundances and spectra from nuclear collisions is motivated by the hope and expectation that in collisions between sufficiently large nuclei at sufficiently high energies a state of excited nuclear matter close to local thermodynamic equilibrium can be formed, allowing us to study the thermodynamics of QCD and the possible phase transition from a HG to a QGP at a critical energy density. Since we do not yet reliably know how big the collision system and how large the beam energy has to be for this to occur (if at all), thermal models should be considered as a phenomenological tool to test for such a behavior. Even if successful, the validity of such an approach must be checked later by a more detailed theoretical analysis of the kinetic evolution of the collision fireball.

It has been noted repeatedly that, especially in collisions involving heavy nuclear targets, the observed particle spectra, after correcting for resonance decay effects [17], resemble thermal distributions with a common temperature T (although a flow component cannot presently be excluded and is actually quite likely [9]), and that so far the interpretation in terms of a generalized thermal model, which assumes equilibration only of the momentum distributions and the light quark abundances, but allows for deviations in particle abundances from *absolute chemical* equilibrium, in particular in the strange sector, appears to be consistent with the observed particle ratios [2]. In this section we will discuss this model as far as it is relevant for our analysis.

2.1 Fireball parameters

Let us assume that in collisions between two nuclei a region with nearly thermal equilibrium conditions is formed near “central” rapidity, *i.e.* at rest in the center of momentum frame of the projectile and a target tube with the diameter of the projectile.

This central fireball from which the observed particles emerge is described by its temperature T and by the chemical potentials μ_i of the different conserved quark flavors u, d, s . Since the conserved quantum numbers of hadrons are simply the sum of the corresponding quantum numbers of their quark constituents, the hadronic chemical potentials are given as the sum of constituent quark chemical potentials. Since the strong and electromagnetic interactions do not mix quark flavors, u, d , and s quarks are separately conserved on the time scale of hadronic collisions, and they can only be produced (or annihilated) in pairs: $X \leftrightarrow q_i \bar{q}_i$. This implies that in *absolute chemical equilibrium* the chemical potentials for par-

ticle and anti-particle flavors are opposite to each other. This observation can be restated in terms of the particle fugacities which are convenient for counting particles and are related to the chemical potentials by:

$$\lambda_i = e^{\mu_i/T} . \quad (1)$$

Since the quantum numbers of a hadron are simply the sum of the corresponding quantum numbers of their constituent quarks, the fugacity of each HG species is simply the product of the quark fugacities, *viz.* $\lambda_p = \lambda_u^2 \lambda_d$, $\lambda_{K^+} = \lambda_u \lambda_{\bar{s}}$, etc. Consequently the relation between particle and anti-particle fugacity is in general:

$$\lambda_{\bar{i}} = \lambda_i^{-1} . \quad (2)$$

If absolute equilibrium is not reached, this relationship can still be maintained by introducing an additional parameter characterizing the approach to equilibrium. For strange particles, specifically, absolute chemical equilibrium is not easy to obtain: due to the higher mass threshold, the production of $\bar{s}s$ pairs usually proceeds much more slowly than that of $\bar{u}u$ and $\bar{d}d$ pairs. This is true both in hadronic interactions and in the quark-gluon plasma [13]. In fact, the $s\bar{s}$ equilibration time scale is estimated to be of the same order of magnitude as the total lifetime of the collision fireball in the QGP phase [18], and much longer than that in the hadronic phase [19]. On the other hand, once a certain number of strange-anti-strange pairs has been created in such a hadron gas, their redistribution among the various strange hadronic species is no longer hindered by any thresholds and occurs relatively fast. It thus makes sense to introduce the concept of *relative chemical equilibrium*, in which the strange phase space is not fully saturated, but whatever strangeness has already been created is distributed among the available strange hadron channels according to the law of maximum entropy. Parametrizing the approach to strange phase space saturation by a factor $0 < \gamma_s \leq 1$, the individual hadron fugacities are then given by

$$\gamma_i \lambda_i \equiv \gamma_s^{n(i,s)} \lambda_i , \quad (3)$$

where the λ_i still satisfy the chemical equilibrium condition (2), and where the power $n(i, s)$ counts the total number of strange valence quarks *plus* anti-quarks in hadron species i .

Altogether, within the thermal model the fireball is thus described by 5 parameters: its temperature T , its baryon chemical potential

$$\mu_B = 3\mu_q , \quad (4)$$

the strangeness chemical potential μ_s , the light quark asymmetry potential $\delta\mu$ (see subsection 2.2) and the strangeness saturation factor γ_s . The value of the temperature can be extracted from the observed transverse momentum spectra whose exponential slope is governed by a combination of thermal motion and collective expansion of the fireball [9]. The separation of these two contributions, *i.e.* the isolation of T , is not straightforward, but has been studied extensively in [9]. Given T , the number of independent variables is further reduced by studying the u - d asymmetry in the fireball and relating it to the asymmetry potential $\delta\mu$, and by the condition of strangeness conservation. This leaves us with two independent variables, say μ_B and γ_s , which have to be determined from measured particle ratios.

The various parameters described above enter the thermodynamic description through the partition function from which all observables are derived. For the hadronic gas state we follow here the conventional hadronic gas model first developed by Hagedorn [20] in which the equation of state of any hadronic system is obtained from a partition function which sums over all hadronic resonances. It is believed that by including a complete set of intermediate scattering states in the form of (usually zero-width) hadronic resonances the dominant interactions within the hadronic system are automatically taken into account. However, an important but tacit approximation is made in this approach, concerning the parameters such as mass (and sometimes widths) of the resonances which are inserted with their free space values. This neglects the possibility that in particular at high temperature and particle or baryon density, there may occur significant shifts from the free space values— one often speaks in this context of the melting of hadronic masses as one approaches extreme conditions. While we do our computations entirely within the conservative framework of the conventional model, our general physics discussion will be shaped in such a way that our conclusions should not critically depend on the exact validity of the model used.

The standard hadronic gas model is certainly not sufficiently precise for our purpose if we were to ask questions concerning the absolute values of energy, entropy, baryon density, etc. which depend either on the ever increasing mass spectrum of particles or on the proper volume occupied by the particles [21]. However, the condition of zero strangeness and quantities such as the entropy per baryon, which involve ratios of extensive variables, are independent of the absolute normalization of the volume and of the renormalization introduced by the diverging particle spectrum and hence can safely be considered in our approach.

We now turn to the discussion of the constraints which limit the number of the free thermal parameters in the fireball.

2.2 u - d asymmetry

In our calculations we will distinguish between the u and d quarks by introducing separate fugacities, λ_u and λ_d , instead of λ_q in the partition function. Since even in the heaviest nuclei there is only a small u - d asymmetry due to the neutron excess, we find it convenient to work with the variables:

$$\mu_q = (\mu_d + \mu_u)/2 , \quad (5)$$

$$\delta\mu = \mu_d - \mu_u . \quad (6)$$

Here, μ_q is the “light quark” chemical potential ($\mu_B/3$ in terms of the baryochemical potential) and $\delta\mu$ describes the asymmetry in the number of up and down quarks due to the neutron excess in the heavy ion collision. The ratio of the net number of down and up quarks in the fireball is

$$R_f = \frac{\langle d - \bar{d} \rangle}{\langle u - \bar{u} \rangle} . \quad (7)$$

In a central S-W collisions, where a tube with the transverse area of the S projectile is swept out from the W target and participates in the fireball $R_f^{S-W} \simeq 1.08$; in Pb-Pb collisions $R_f^{Pb-Pb} = 1.15$. The value of $\delta\mu$ is at each fixed T determined by the value of R_f , but depends on the assumed structure of the source, *i.e.* the EoS. We have investigated this relation for the two cases considered here: the conventional HG and the QGP.

In the HG phase we include in the partition function all non-strange mesons up to a mass of 1690 MeV, all nucleons up to 1675 MeV and all Δ 's up to 1900 MeV. [We note that higher resonances would matter only if their number were divergent (as is the case in the Bootstrap approach of Hagedorn [20]) and if the HG was sufficiently long lived to populate all high mass resonances]. In addition strange hadrons are included as described in Eq. (10) below, which we expand in calculations to allow to distinguish between u and d quarks within the various strange hadron multiplets.

In Fig. 1 we show how in the conventional hadron gas the difference $\delta\mu/\mu_q$ induced by the isospin asymmetry of the fireball depends on the temperature, for two selected values $R_f = 1.08$ and 1.15 (appropriate for S–W and Pb–Pb collisions, respectively), and for three fixed values of $\lambda_s = 0.95, 1.00$, and 1.05 . The curves shown correspond to non-trivial solutions (*i.e.* solutions with $\mu_q \neq 0$) of the strangeness balance equation with the given values for λ_s ; as we will explain below, these solutions cease to exist (since we require $\langle s - \bar{s} \rangle \simeq 0$) above a certain critical temperature, which is given by $T \simeq 230$ MeV for $\lambda_s = 1$ and smaller (larger) for smaller (larger) values of λ_s . We see that, while for $T \rightarrow 0$ the ratio $\delta\mu/\mu_q$ vanishes in the hadron gas, it is of the same order as the deviation from unity of R_f once T reaches values around 200 MeV which are of interest here.

For the QGP the ratio $\delta\mu/\mu_q$ is independent of λ_s , due to the decoupling of the strange and non-strange chemical potentials in the partition function. For $\mu_q < \pi T$ one finds [3]

$$R_f^{\text{QGP}} \simeq \frac{\mu_d}{\mu_u} \simeq 1 + \frac{\delta\mu}{\mu_q}, \quad (8)$$

such that $\delta\mu/\mu_q$ is exactly equal to $R_f - 1$. It is remarkable that towards the maximum temperature consistent with strangeness conservation the HG and QGP based results for $\delta\mu$ at a given R_f nearly agree. We thus find that, although small, the difference between the chemical potentials of u and d quarks is not always negligible. We note for later applications that in the region of interest to us here ($T \sim 210$ MeV) we have irrespective of the nature of the fireball:

$$\frac{\delta\mu}{T} \approx \frac{\mu_q}{T} (R_f - 1). \quad (9)$$

2.3 The strangeness partition function

In the Boltzmann approximation, it is easy to write down the partition function for the strange particle fraction of the hadronic gas, \mathcal{Z}_s , and we follow the notation of Ref. [14].

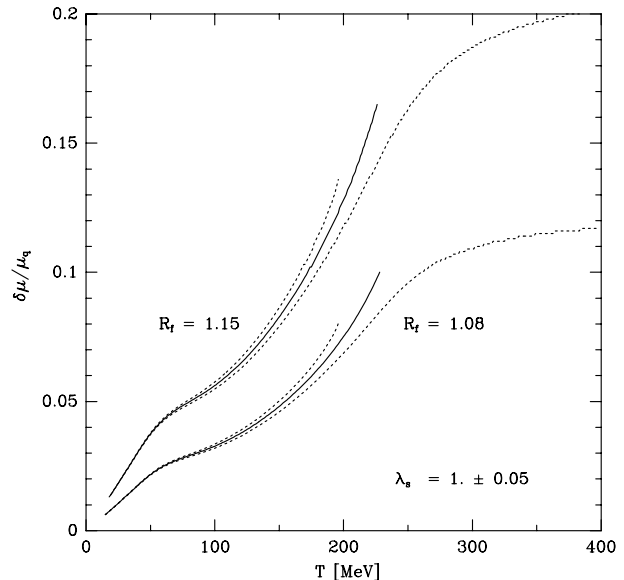


Figure 1: $\delta\mu/\mu_q$ asymmetry for $R_f = 1.08$ (S–W collisions) and $R_f = 1.15$ (Pb–Pb collisions). Solid lines: $\lambda_s = 1.00$; upper dotted lines: $\lambda_s = 0.95$; lower dotted lines: $\lambda_s = 1.05$.

However, given the recently measured values of the thermal parameters (which allow in particular for a rather high temperature $T \sim 210$ MeV) it is necessary to sum over some more strange hadronic particles than was done in Eq. (7) of Ref. [14]. Including the possibility of only partially saturated strange phase space through the factor γ_s above, but neglecting for the moment the isospin asymmetry $\delta\mu$, we have:

$$\ln \mathcal{Z}_s^{\text{HG}} = \frac{V_h T^3}{2\pi^2} \left[(\lambda_s \lambda_q^{-1} + \lambda_s^{-1} \lambda_q) \gamma_s F_K + (\lambda_s \lambda_q^2 + \lambda_s^{-1} \lambda_q^{-2}) \gamma_s F_Y \right. \\ \left. + (\lambda_s^2 \lambda_q + \lambda_s^{-2} \lambda_q^{-1}) \gamma_s^2 F_\Xi + (\lambda_s^3 + \lambda_s^{-3}) \gamma_s^3 F_\Omega \right] \quad (10)$$

where the kaon (K), hyperon (Y), cascade (Ξ) and omega (Ω) degrees of freedom in the hadronic gas are included successively. The phase space factors F_i of the various strange particles are:

$$F_K = \sum_j g_{K_j} W(m_{K_j}/T); \quad K_j = K, K^*, K_2^*, \dots, \quad m \leq 1650 \text{ MeV}, \\ F_Y = \sum_j g_{Y_j} W(m_{Y_j}/T); \quad Y_j = \Lambda, \Sigma, \Sigma(1385), \dots, \quad m \leq 1750 \text{ MeV}, \\ F_\Xi = \sum_j g_{\Xi_j} W(m_{\Xi_j}/T); \quad \Xi_j = \Xi, \Xi(1530), \dots, \quad m \leq 1820 \text{ MeV}, \\ F_\Omega = \sum_j g_{\Omega_j} W(m_{\Omega_j}/T); \quad \Omega_j = \Omega. \quad (11)$$

where the g_i are the spin-isospin degeneracy factors, $W(x) = x^2 K_2(x)$, and K_2 is the modified Bessel function.

For the quark-gluon plasma, on the other hand, the strange contribution to the partition function is much simpler, because the strange quarks and anti-quarks are isolated and do not occur in clusters with non-strange quarks as in the hadron gas:

$$\ln \mathcal{Z}_s^{\text{QGP}} = \frac{g_s V T^3}{2\pi^2} \int p^2 dp \left[\ln \left(1 + \gamma_s \lambda_s e^{-\sqrt{m_s^2 + p^2}/T} \right) + \ln \left(1 + \gamma_s \lambda_s^{-1} e^{-\sqrt{m_s^2 + p^2}/T} \right) \right]. \quad (12)$$

with the strange quark spin-color degeneracy factor

$$g_s = 2 \times 3 = 6. \quad (13)$$

For the value of the strange quark mass we take $m_s \sim 150$ – 180 MeV; in Eq. (12) γ_s and λ_s do not factorize as has been the case for the hadron gas, because T is of order m_s and the Boltzmann approximation is not always satisfactory and can produce errors of the order of 20%. Recall that in general the strange particle density in a QGP is larger by a factor 2–5 than in a HG, due to the lower threshold ($m_s < m_K$) and the presence of the color degeneracy factor in Eq. (13).

2.4 Strangeness balance

We will now discuss the reduction of the number of free parameters caused by the condition of strangeness balance. Since the net strangeness of the colliding nuclei in the initial state is

zero, and strangeness is conserved by strong interactions, the net strangeness of the collision fireball will stay close to zero throughout the collision, except for corrections due to possible strangeness asymmetry in pre-equilibrium and asymmetric surface radiation of strange hadrons [22]. If these processes can be neglected, the resulting condition of vanishing total strangeness takes the form

$$0 = \rho_s = \langle s \rangle - \langle \bar{s} \rangle = \lambda_s \frac{\partial}{\partial \lambda_s} \ln \mathcal{Z}_s, \quad (14)$$

where ρ_s is the net strangeness density,

$$\rho_s = \sum_i s_i \rho_i, \quad (15)$$

with s_i being the strangeness of particle species i having density ρ_i , and the sum going over all particle species i existing in the respective phase (QGP or HG). While for the QGP this relation leads always to the result $\lambda_s = 1$ or $\mu_s = 0$ (as one easily verifies by inserting Eq. (12)), for the hadron gas it is an implicit equation relating λ_s to λ_q in a way which depends on the temperature T [14, 23].

In order to also be able to account for pre-equilibrium and surface emission fluctuations, we introduce the net strangeness fraction

$$\varepsilon \equiv \frac{\langle \bar{s} \rangle - \langle s \rangle}{\langle s \rangle}, \quad (16)$$

and will also consider solutions for the analogue of Eq. (14), where the left hand side is given by $-\varepsilon \langle s \rangle$. In this work we restrict ourselves to asymmetries $|\varepsilon| \leq 0.1$ which might be accessible by purely statistical fluctuations caused by surface emission, without “strangeness distillation” during QGP hadronization [23, 22] which arises when chemical equilibrium is enforced during a slow QGP hadronization process. An analysis of the phase diagram and the strangeness balance conditions for systems with very large net strangeness is presented elsewhere [24]. We note briefly the practical consequences of $\varepsilon = \pm 0.1$: for the fireball created in central S–W collisions one has about 108 baryons in the interaction tube. If we consider a hadron gas with the thermal parameters (without flow component) as determined for these S–W collision data [6], we find a strange pair abundance of about 0.4 per baryon or about 40 strange pairs in total. The maximum asymmetry considered here in the HG phase at $T \simeq 200$ MeV is thus about ± 4 strange quarks. Fluctuations of this magnitude are expected to occur in about half of the collision systems.

2.4.1 The case $\mu_s = 0$ ($\lambda_s = 1$)

Since the vanishing of μ_s for all values of T and μ_B in a strangeness neutral QGP appears to be such a unique feature of this state, it is interesting to ask to what extent this condition could arise in a HG. We will therefore first study the mechanisms which lead in a HG model to a small strange quark chemical potential in a restricted region of temperatures. Of course, for a baryon-free system ($\mu_B = 0$) even in the hadron gas $\mu_s = 0$ is a natural consequence of strangeness neutrality. For systems with non-vanishing baryon number (like the central rapidity fireballs created at AGS and SPS energies) this is no longer true. We therefore

ask ourselves under which conditions $\mu_s = 0$, *viz.* $\lambda_s = 1$, allows for non-zero values of μ_B^0 to be consistent with strangeness neutrality. This question can be answered analytically: inserting the partition function (10) into the strangeness neutrality condition (14), we see that at $\lambda_s = 1$ the phase space for Ω and $\bar{\Omega}$ cancels out, giving the exact result

$$\mu_B^0 = 3 \cosh^{-1} \left(\frac{F_K}{2F_Y} - \gamma_s \frac{F_\Xi}{F_Y} \right). \quad (17)$$

There is a real solution only when the argument on the right hand side is larger than unity. It turns out that this condition is a sensitive function of the temperature T and of the hadronic resonances included (and therefore of the masses of the resonances). In particular, for any given resonance mass spectrum used to compute the phase space factors F_i , there is a temperature T_0 beyond which no such solution is possible — this occurs since F_K/F_Y is a monotonically decreasing function of T (see Fig. 1 in Ref. [14]).

The case of exact strangeness neutrality ($\varepsilon = 0$) in a HG in absolute chemical equilibrium ($\gamma_s = 1$) was considered in [7], and for this choice of parameters our following theoretical analysis essentially agrees with that work.

2.4.2 HG behavior of μ_s and μ_B for nearly conserved strangeness

An important aspect to consider is the value of μ_s observed and how it is compatible with the picture of the reaction. The reason that μ_s is of such importance is the expected value $\mu_s = 0$ associated with QGP. We first will address the question under what circumstances this value is accessible to a HG fireball, and then turn to discuss more generally how different dynamical scenarios can be distinguished. We expect that there is a domain of temperatures for which even a considerable change of μ_B between $\mu_B = 0$ and μ_B^0 does not induce a significant change of μ_s .

For the extensive set of resonances included here this quite peculiar behavior occurs at $T \simeq 210$ MeV for $\varepsilon = 0$ and at $T \simeq 200$ MeV for $\varepsilon = -0.1$. In Figs. 2a, 2b, 2c we present the constraint between μ_s and μ_B at fixed $T = 200$ MeV (solid curves), 150 MeV (long-dashed curves), 300 MeV (short-dashed curves) and 1000 ($\simeq \infty$) MeV (dotted curves) for $\varepsilon = 0$ (Fig. 2a), $\varepsilon = 0.1$ (Fig. 2b), and $\varepsilon = -0.1$ (Fig. 2c), all for $\gamma_s = 0.7$. The choice $\gamma_s = 1$ would not change our results significantly. The flat behavior of μ_s as a function of μ_B for $\varepsilon = 0$ and $T \simeq 200$ MeV makes it hard to distinguish the hadron gas from a QGP (which has $\mu_s \equiv 0$ independent of μ_B) in this temperature range. This was pointed out in Ref. [7], but we think that Eq. (17) and the corresponding Fig. 2a, with our definition of μ_s (see footnote 1), exhibits this effect more clearly and allows us to understand the accidental nature of this behavior.

For $\varepsilon = 0$ (Fig. 2a) all curves pass through $\mu_s = 0$ at $\mu_B = 0$, and as $T \rightarrow \infty$ one approaches a limiting curve which is rather well represented by the dotted curve corresponding to 1000 MeV. For $\varepsilon \neq 0$ we note that in the QGP phase the strange quark chemical potential does not vanish (see horizontal lines in Figures 2b, 2c), and that there is a common crossing region of the HG and QGP results at a finite value of μ_s , close to $\mu_B = 0$. For $T \rightarrow \infty$ for a fixed positive (negative) net strangeness fraction ε , μ_s continues to increase (decrease) at fixed μ_B as a function of T , and only the slope as a function of μ_B approaches a definite limit as $T \rightarrow \infty$.

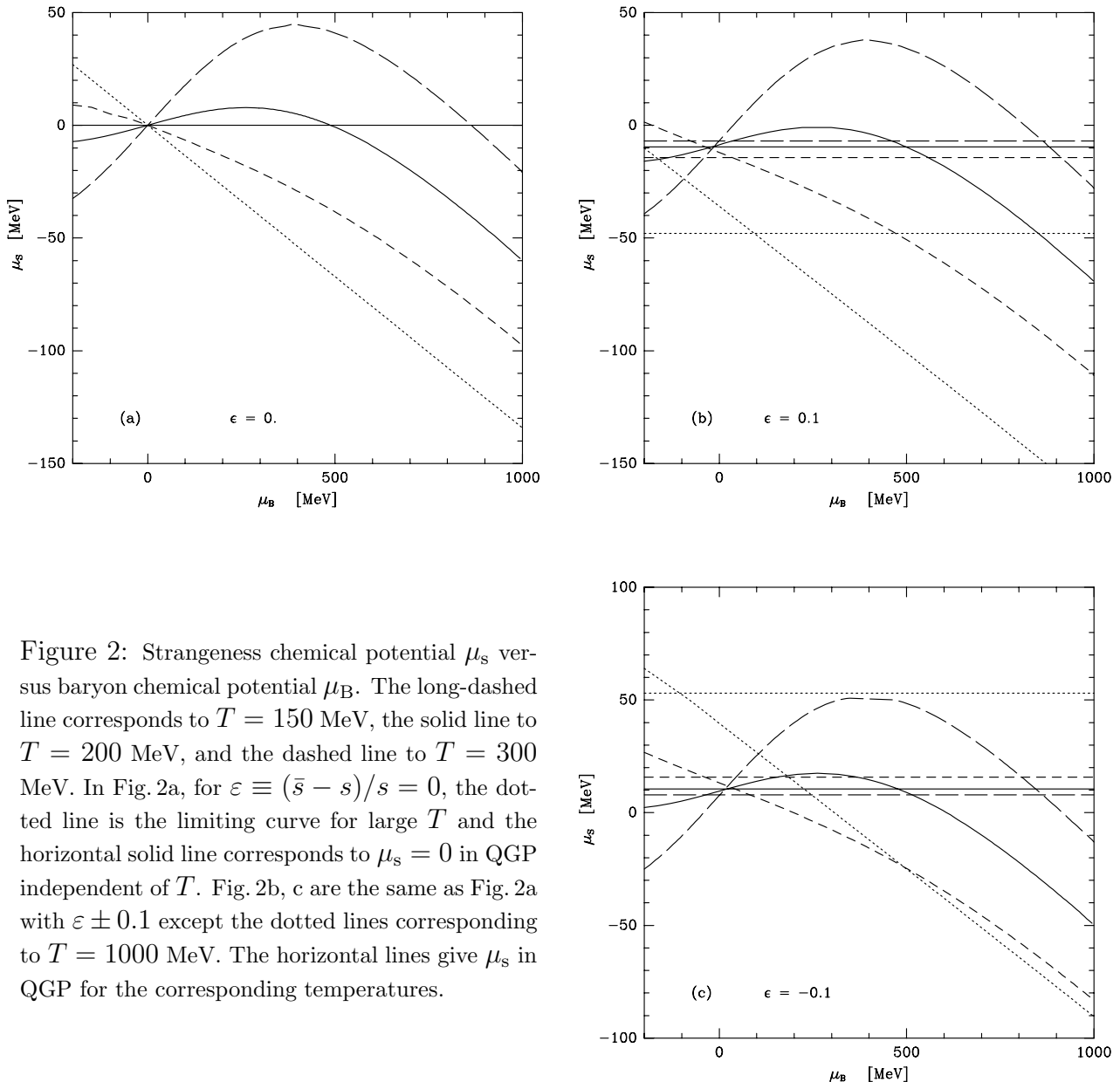


Figure 2: Strangeness chemical potential μ_s versus baryon chemical potential μ_B . The long-dashed line corresponds to $T = 150$ MeV, the solid line to $T = 200$ MeV, and the dashed line to $T = 300$ MeV. In Fig. 2a, for $\varepsilon \equiv (\bar{s} - s)/s = 0$, the dotted line is the limiting curve for large T and the horizontal solid line corresponds to $\mu_s = 0$ in QGP independent of T . Fig. 2b, c are the same as Fig. 2a with $\varepsilon \pm 0.1$ except the dotted lines corresponding to $T = 1000$ MeV. The horizontal lines give μ_s in QGP for the corresponding temperatures.

3 Analysis of the data within the fireball model

In this section we describe, using as an example the experiment with the most detailed information of strange baryon and anti-baryon production, WA85 [26], how to extract estimates of the relevant thermodynamic parameters from particle production data. This procedure is straightforward if one can focus on the ground state baryons of a given flavor content, *i.e.* if the production and decay of heavier resonances can be neglected. Such an analysis was presented in [3, 6], and its essential steps will be shortly repeated in subsections 3.1 through 3.3. If T is indeed in the region of 210 MeV as the m_\perp -slopes seem to indicate, resonance production and decays can, however, not be neglected, and therefore such a procedure is not fully consistent. In subsection 3.4 we therefore redo this analysis including resonance decays, which is then much more involved. The main result is that resonance decays mainly affect

the extraction of the strangeness saturation factor γ_s (inclusion of resonance decays drives the extracted γ_s closer to 1, *i.e.* towards full saturation of hadronic gas phase space), while the striking conclusion that the data point towards a vanishing strange chemical potential $\mu_s \approx 0$ is remarkably stable against these corrections.

3.1 Cancellation of the Boltzmann factor

It was argued in [3] that within the thermal model it is quite easy to extract the fugacities from a given particle ratio *at fixed* m_\perp *and* y , thus eliminating the need to extrapolate the experimental data to full phase space. Specifically, for a stationary fireball one finds for the ratio of particles i and j , for each of which the invariant cross section is experimentally known at a certain rapidity $y \pm dy/2$ in the region $m_\perp \geq m_\perp^{\text{cut}}$:

$$\left. \frac{dN_i/dy}{dN_j/dy} \right|_{m_\perp \geq m_\perp^{\text{cut}}} = \frac{g_i \gamma_i \lambda_i \int_{m_\perp^{\text{cut}}}^{\infty} m_\perp \cosh y \exp(-m_\perp \cosh y/T) dm_\perp^2}{g_j \gamma_j \lambda_j \int_{m_\perp^{\text{cut}}}^{\infty} m_\perp \cosh y \exp(-m_\perp \cosh y/T) dm_\perp^2}. \quad (18)$$

Here we used the identity $E = m_\perp \cosh y$ for the particle energy (with y measured relative to the center of mass of the collision fireball) to rewrite the transverse mass integral over the Boltzmann distribution $E \exp(-E/T)$ (the factor E results from starting with the Lorentz-invariant cross section $E d^3N/d^3p$). If the fireball is not stationary, but expands in the longitudinal direction in a boost-invariant way, dN/dy is independent of y , and the factors $E \exp(-E/T)$ under the integrals on the r. h. s. of Eq. (18) have to be replaced by a Bessel function [9]:

$$\frac{dN_i^{\text{thermal}}}{dy dm_\perp^2} = g_i \gamma_i \lambda_i m_\perp K_1 \left(\frac{m_\perp}{T} \right), \quad (19)$$

where we neglected a common normalization constant containing the fireball volume which drops out from the ratio². The important observation is that obviously in both cases the Boltzmann factors (and with them all dependence on the particle rest masses) drop out from the ratio, due to the common lower cutoff on m_\perp (which, of course, must be larger than either rest mass). The same remains true if m_\perp is not integrated over, but the ratio is evaluated at fixed m_\perp . Since the degeneracy factors g_i are known, this immediately yields the ratio of the generalized fugacities $\gamma_i \lambda_i$ (see Eq. (3)).

3.2 Extraction of μ_s and μ_q from anti-baryon data

Thus, comparing the *spectra* of particles with those of their anti-particles within overlapping regions of m_\perp , the Boltzmann and *all* other statistical factors cancel from their relative normalization, which is thus a function of the fugacities only. [In subsection 3.4 we show that this statement, although no longer strictly true, still remains approximately valid when feed-down by resonance decays is included.] For the currently available two such ratios one has specifically

$$R_\Xi = \frac{\overline{\Xi^-}}{\Xi^-} = \frac{\lambda_d^{-1} \lambda_s^{-2}}{\lambda_d \lambda_s^2}, \quad (20)$$

²The same result is obtained if the spectrum in Eq. (18) is integrated over rapidity, *i.e.* if one wants to describe with a stationary fireball data obtained over a large rapidity window.

$$R_\Lambda = \frac{\bar{\Lambda}}{\Lambda} = \frac{\lambda_d^{-1} \lambda_u^{-1} \lambda_s^{-1}}{\lambda_d \lambda_u \lambda_s}. \quad (21)$$

These ratios can easily be related to each other, in a way which shows explicitly the respective isospin asymmetry factors and strangeness fugacity dependence. Eqs.(20, 21) imply:

$$R_\Lambda R_{\Xi}^{-2} = e^{\delta\mu_s/T} \cdot e^{2\delta\mu/T}, \quad (22)$$

$$R_{\Xi} R_\Lambda^{-2} = e^{\delta\mu_q/T} \cdot e^{-\delta\mu/T}. \quad (23)$$

Eqs.(22, 23) are generally valid, irrespective of the state of the system (HG or QGP), as long as the momentum spectra of the radiated particles are thermal with a common temperature. We see that once the left hand side is known experimentally, it determines rather accurately the values of μ_q, μ_s which enter on the right hand side with a dominating factor 6, while the (small) isospin asymmetry $\delta\mu$ plays only a minor role. This explains how, by applying these identities to the WA85 data [26], it has been possible to determine the chemical potentials with considerable precision in spite of the still pretty large experimental errors on the measured values of R_Λ, R_{Ξ} .

Turning to the pertinent experimental results we first recall the recently released data on the rapidity dependence of $\bar{\Lambda}$ and Λ production rates measured by the experiment NA36 [27]. There is a clear indication that the production of these particles in nuclear S–Pb collisions is concentrated in the central rapidity domain — it does not follow in its behavior the FRITIOF simulations which, on the other hand, are consistent with the production rates from p–Pb collisions. This supports the notion of a central fireball reaction picture for S–W collisions studied by WA85 [26]. The most striking result of the latter experiment is the fact that the abundance of charged anti-cascades ($\bar{s}\bar{u}\bar{d}$) is unusually enhanced, in particular when compared to the abundance of cascades (ssd) and anti-lambdas ($\bar{s}\bar{u}\bar{d}$). We now interpret the data in terms of the local equilibrium model, thus fixing the values of μ_s and μ_q .

The $\bar{\Xi}^-/\Xi^-$ ratio has been reported as:

$$R_{\Xi} = 0.39 \pm 0.07 \quad \text{for } y \in (2.3, 3.0) \text{ and } m_\perp > 1.72 \text{ GeV}. \quad (24)$$

Note that, in p–W reactions in the same (p_\perp, y) region, a smaller value for the R_{Ξ} ratio, namely 0.27 ± 0.06 , is found. The $\bar{\Lambda}/\Lambda$ ratio is:

$$R_\Lambda = 0.13 \pm 0.03 \quad \text{for } y \in (2.3, 3.0) \text{ and } m_\perp > 1.72 \text{ GeV}. \quad (25)$$

In Eq.(25), corrections were applied to eliminate hyperons originating from cascade decays, but not those originating from decays of $\Omega \rightarrow \Lambda + \bar{K}$ or $\bar{\Omega} \rightarrow \bar{\Lambda} + K$ which are of little significance for the high m_\perp considered here. The ratio R_Λ for S–W collisions is slightly smaller than for p–W collisions in the same kinematic range.

From these two results, together with Eqs.(22, 23, 9) and the value $R_f = 1.08$ mentioned after Eq.(7), we obtain the following values of the chemical potentials for S–W central collisions at 200 GeV A:

$$\frac{\mu_q}{T} = \frac{\ln R_{\Xi}/R_\Lambda^2}{5.92} = 0.53 \pm 0.1, \quad (26)$$

$$\frac{\delta\mu}{T} = \frac{\mu_q}{T}(R_f - 1) = 0.042 \pm 0.008, \quad (27)$$

$$\frac{\mu_s}{T} = \frac{\ln R_\Lambda/R_\Xi^2 - 0.084}{6} = -0.018 \pm 0.05. \quad (28)$$

A study of the temperature observed in these collisions was recently made [8]. As noted in [6] and discussed below in section 4, the possibility of a HG interpretation of these data only poses itself if the transverse mass slope of the produced particles is entirely due to the thermal motion. Under this assumption the temperature is $T = 210 \pm 10$ MeV, and therefore we have:

$$\mu_B = 335 \pm 25 \text{ MeV}, \quad \delta\mu = 9 \pm 2 \text{ MeV}, \quad \mu_s = -3.8 \pm 10 \text{ MeV}. \quad (29)$$

The last result translates into the value $\lambda_s = 0.98 \pm 0.05$ for the strange quark fugacity. Much of what we do later in this paper will rest on this stunning result that the strange chemical potential is very small and perfectly compatible with zero. In our calculations below we will thus consider in particular a HG constrained to this range of values (as well as to near strangeness neutrality).

3.3 Determination of γ_s

A complete cancellation of the fugacity factors occurs when we form the product of the abundances of baryons and anti-baryons. We further can take advantage of the cancellation of the Boltzmann factors by comparing this product for two different particle kinds, *e.g.* we consider:

$$\Gamma_s \equiv \frac{\Xi^-}{\Lambda} \cdot \frac{\overline{\Xi^-}}{\overline{\Lambda}} \Big|_{m_\perp > m_\perp^{\text{cut}}}. \quad (30)$$

If the phase space of strangeness, like that of the light flavors, were fully saturated, the fireball model would imply $\Gamma_s = 1$. However, any deviation from absolute chemical equilibrium as expressed by the factor γ_s will change the value of Γ_s . Ignoring as before any feed-down effects from higher resonances we find

$$\Gamma_s = \gamma_s^2. \quad (31)$$

In principle the measurement of γ_s can be done with other particle ratios; in the absence of resonance feed-down we have

$$\gamma_s^2 = \frac{\Lambda}{p} \cdot \frac{\overline{\Lambda}}{\overline{p}} \Big|_{m_\perp > m_\perp^{\text{cut}}} = \frac{\Xi^-}{\Lambda} \cdot \frac{\overline{\Xi^-}}{\overline{\Lambda}} \Big|_{m_\perp > m_\perp^{\text{cut}}} = \frac{\Omega^-}{2\Xi^-} \cdot \frac{\overline{\Omega^-}}{2\overline{\Xi^-}} \Big|_{m_\perp > m_\perp^{\text{cut}}}, \quad (32)$$

where in the last relation the factors 2 in the denominator correct for the spin-3/2 nature of the Ω . As we will see in subsection 3.5, Eq. (51), these double ratios are considerably affected by resonance decays.

We note that in the kinematic domain of Eqs. (24, 25) the experimental results reported by the WA85 collaboration are:

$$\frac{\overline{\Xi^-}}{\overline{\Lambda + \Sigma^0}} = 0.6 \pm 0.2, \quad \frac{\Xi^-}{\Lambda + \Sigma^0} = 0.20 \pm 0.04. \quad (33)$$

If the mass difference between Λ and Σ^0 is neglected, this implies in the framework of the thermal model that an equal number of Λ 's and Σ^0 's are produced, such that

$$\frac{\overline{\Xi^-}}{\overline{\Lambda}} = 1.2 \pm 0.4, \quad \frac{\Xi^-}{\Lambda} = 0.40 \pm 0.08. \quad (34)$$

The fact that the more massive and stranger anti-cascade exceeds at fixed m_\perp the abundance of the anti-lambda is most striking. These results are inexplicable in terms of simple cascade models for the heavy-ion collision [28]. The relative yield of $\overline{\Xi^-}$ appears to be 5 times greater than seen in the p - p ISR experiment [29] and all other values reported in the literature [26].

Combining the experimental result Eq. (34) with Eqs. (30, 31), we find the value

$$\gamma_s = 0.7 \pm 0.1. \quad (35)$$

3.4 Temperature, transverse mass spectrum

The data from the WA85 collaboration [26] correspond to an apparent temperature (from the slope of the m_\perp -spectra) of $T_{\text{apparent}} = 210 \pm 10$ MeV [8]. In our numerical studies we therefore concentrated on two extreme cases:

- i) $T = 210$ MeV, $\beta_\perp = 0$ (no transverse flow), which we call the ‘‘thermal’’ scenario,
- ii) $T = 150$ MeV, $\beta_\perp = 0.32$, which we call the ‘‘flow’’ scenario for which the freeze-out temperature has been estimated following the results of [9].

If the slope of the experimental spectra is not entirely due to thermal motion, but contains a flow component due to collective expansion of the emitting source [9], then ‘‘flow spectra’’ (*i.e.* boosted Boltzmann spectra) have to be used in the numerator and denominator of Eq. (18). If the flow is azimuthally symmetric and boost-invariant in the longitudinal direction, the thermal spectrum (19) has to be replaced by (again neglecting a common normalization constant)

$$\frac{dN_i^{\text{flow}}}{dy dm_\perp^2} = g_i \gamma_i \lambda_i m_\perp K_1 \left(\frac{m_\perp \cosh \rho}{T} \right) I_0 \left(\frac{p_\perp \sinh \rho}{T} \right), \quad (36)$$

where K_1 and I_0 are the modified Bessel functions and

$$\rho = \tanh^{-1} \beta_f \quad (37)$$

is the transverse flow rapidity. This spectrum has an asymptotic slope corresponding to an apparent ‘‘blue-shifted’’ temperature

$$T_{\text{apparent}} = T \sqrt{\frac{1 + \beta_f}{1 - \beta_f}}. \quad (38)$$

The same result as in Eq. (36) is obtained if the spectrum from a spherically expanding fireball is integrated over rapidity. Since some longitudinal flow is likely to be present in S-W collisions, and also the kinematic window of the WA85 experiment is nearly one unit

of rapidity, we think that the form (36), in which integration over a large rapidity window is implied, is most appropriate for an analysis of the experimental spectra. (The “large window” combines the one unit of y -acceptance in WA85 with about 1.5 units of flow expected [9] for this system.)

Obviously, through the separate dependence on m_{\perp} and p_{\perp} Eq. (36) depends on the particle rest mass explicitly. This spoils the cancellation of the spectral shape from the m_{\perp} -integrated particle ratios as well as their independence from the m_{\perp} -cut, and thus also renders the extraction of the fugacities, etc. more complicated.

In order to assess the importance of these effects we devote next subsection to a more complex reanalysis of the experimentally measured strange baryon and anti-baryon ratios which takes all these complications into account. Anticipating this development we show in Fig. 3 the m_{\perp} -spectra of the various particle species, for both the “thermal” scenario (Figs. 3a, b) and the “flow” scenario (Figs. 3c, d). Dashed lines indicate the direct thermal contribution to the spectra, while the solid lines include all resonance decay contributions (see following subsection). These results allow to directly assess the importance of resonance decays on the m_{\perp} -slopes of the observed particles and on the particle ratios. For the Ω there are no resonance contributions, due to the imposed mass cutoff in the resonance spectrum. While the overall normalization of the spectra is arbitrary, their relative normalization is according to the fugacities given in Table 1.

The presence of flow affects the spectra mostly at low m_{\perp} near the mass threshold [9], where it leads to a flattening, *i.e.* to a higher apparent temperature. The effect is proportional to the particle mass (since for small p_{\perp} the effect of flow can be estimated by $p_{\text{flow}} \simeq m_0 v_{\text{flow}}$) and thus most clearly seen in the Ξ^{-} and Ω spectra.

3.5 Resonance decays

As already mentioned, Eq. (18) is only correct if feed-down to the observed particles by strong decays of higher resonances is neglected. At temperatures of order 200 MeV these resonance decays can no longer be totally ignored. This has two annoying consequences: first, since the decay products have a steeper m_{\perp} -spectrum than the original resonances [17], the various contributions to numerator and denominator in (18) have different slopes, and the integrals over the Boltzmann factors no longer cancel exactly. Second, since different sets of resonances contribute to i and j , the ratio is modified by an a priori unknown factor which turns out to be hard to calculate and in general *does* depend on the experimental m_{\perp} -cutoff as well as on the temperature.

Since the decay spectra drop more steeply as a function of m_{\perp} than the thermal ones, the role of resonance feed-down can in principle be suppressed by going to sufficiently large m_{\perp} . For pions and kaons, for example, the thermal contribution dominates for $m_{\perp} > 1\text{--}1.5$ GeV, in spite of the huge contribution of decay pions to the total yield [17]; the latter all end up at lower m_{\perp} . For baryons due to their larger masses, the difference in slope between the thermal and decay baryons is less drastic, and one has to go to still larger m_{\perp} before the resonance decay contributions are sufficiently suppressed.

Including resonance decays, the numerator and denominator of Eq. (18) take the form

$$\frac{dN_i}{dy} \Big|_{m_{\perp} \geq m_{\perp}^{\text{cut}}} = \int_{m_{\perp}^{\text{cut}}}^{\infty} dm_{\perp}^2 \left\{ \frac{dN_i^{\text{thermal/flow}}(T)}{dy dm_{\perp}^2} + \sum_R b_{R \rightarrow i} \frac{dN_i^R(T)}{dy dm_{\perp}^2} \right\}, \quad (39)$$

with the direct thermal or flow contribution given by (19) or (36), respectively, and the contribution from decays of resonances $R \rightarrow i + 2 + \dots + n$ (with branching ratio $b_{R \rightarrow i}$ into the observed channel i) calculated according to [17]

$$\frac{dN_i^R}{dy dm_{\perp}^2} = \int_{s_-}^{s_+} ds g_n(s) \int_{Y_-}^{Y_+} dY \int_{M_{\perp}^-}^{M_{\perp}^+} dM_{\perp}^2 \quad (40)$$

$$\frac{M}{\sqrt{P_{\perp}^2 p_{\perp}^2 - [ME^* - M_{\perp} m_{\perp} \cosh(Y - y)]^2}} \left(\frac{dN_R}{dY dM_{\perp}^2} \right).$$

Capital letters indicate variables associated with the resonance R , \sqrt{s} is the invariant mass of the unobserved decay products $2, \dots, n$, and the kinematic limits are given by

$$s_{\pm} = \left(\sum_{k=2}^n m_k \right)^2, \quad s_{+} = (M - m_i)^2, \quad (41)$$

$$Y_{\pm} = y \pm \sinh^{-1} \frac{p^*}{m_{\perp}}, \quad (42)$$

$$M_{\perp}^{\pm} = M \frac{E^* m_{\perp} \cosh(Y - y) \pm p_{\perp} \sqrt{p^{*2} - m_{\perp}^2 \sinh^2(Y - y)}}{m_{\perp}^2 \sinh^2(Y - y) + m_i^2}, \quad (43)$$

$$E^* = \frac{1}{2M} (M^2 + m_i^2 - s), \quad p^* = \sqrt{E^{*2} - m_i^2}. \quad (44)$$

In (40) $g_n(s)$ is the decay phase space for the n -body decay $R \rightarrow i + 2 + \dots + n$, and for the dominant 2-body decay (assuming isotropic decay in the resonance rest frame) it is given by

$$g_2(s) = \frac{1}{4\pi p^*} \delta(s - M^2), \quad (45)$$

for $n > 2$ see Ref. [17].

The resonance spectrum $dN_R/dY dM_{\perp}^2$ entering the r. h. s. of Eq. (40) is in general itself a sum of a thermal or flow spectrum like (19) or (36) and of decay spectra from still higher lying resonances; for example, most decays of high-lying nucleon resonances into protons or anti-protons proceed through the $\Delta(1232)$ or its anti-particle (*e.g.* $N(1440) \rightarrow \Delta(1232) + \pi \rightarrow p + 2\pi$). This has been taken into account in our calculations. Extracting the degeneracy factors and fugacities of the decaying resonances, we write shortly

$$N_i^R \equiv \gamma_R \lambda_R \tilde{N}_i^R \equiv \gamma_R \lambda_R \int_{m_{\perp}^{\text{cut}}}^{\infty} dm_{\perp}^2 \sum_R g_R b_{R \rightarrow i} \frac{d\tilde{N}_i^R}{dy dm_{\perp}^2}, \quad (46)$$

with the sum now including only resonances with identical quantum numbers; if these quantum numbers agree with those of species i , the sum is meant to also include the thermal contribution.

Between particles and anti-particles we have the relation

$$N_i^{\bar{R}} = \gamma_R \lambda_R^{-1} \tilde{N}_i^R = \lambda_R^{-2} N_i^R. \quad (47)$$

The three independent particle ratios measured by WA85 [26] are thus given by

$$R_{\Xi} = \frac{\overline{\Xi^-}}{\Xi^-} \Big|_{m_{\perp} \geq m_{\perp}^{\text{cut}}} = \frac{\gamma_s^2 \lambda_q^{-1} \lambda_s^{-2} \tilde{N}_{\Xi}^{\Xi^*} + \gamma_s^3 \lambda_s^{-3} \tilde{N}_{\Xi}^{\Omega^*}}{\gamma_s^2 \lambda_q \lambda_s^2 \tilde{N}_{\Xi}^{\Xi^*} + \gamma_s^3 \lambda_s^3 \tilde{N}_{\Xi}^{\Omega^*}}, \quad (48)$$

$$R_{\Lambda} = \frac{\overline{\Lambda}}{\Lambda} \Big|_{m_{\perp} \geq m_{\perp}^{\text{cut}}} = \frac{\gamma_s \lambda_q^{-2} \lambda_s^{-1} \tilde{N}_{\Lambda}^{Y^*} + \gamma_s^2 \lambda_q^{-1} \lambda_s^{-2} \tilde{N}_{\Lambda}^{\Xi^*} + \gamma_s^3 \lambda_s^{-3} \tilde{N}_{\Lambda}^{\Omega^*}}{\gamma_s \lambda_q^2 \lambda_s \tilde{N}_{\Lambda}^{Y^*} + \gamma_s^2 \lambda_q \lambda_s^2 \tilde{N}_{\Lambda}^{\Xi^*} + \gamma_s^3 \lambda_s^3 \tilde{N}_{\Lambda}^{\Omega^*}}, \quad (49)$$

$$R_s = \frac{\Xi^-}{\Lambda} \Big|_{m_{\perp} \geq m_{\perp}^{\text{cut}}} = \frac{\gamma_s^2 \lambda_q \lambda_s^2 \tilde{N}_{\Xi}^{\Xi^*} + \gamma_s^3 \lambda_s^3 \tilde{N}_{\Xi}^{\Omega^*}}{\gamma_s \lambda_q^2 \lambda_s \tilde{N}_{\Lambda}^{Y^*} + \gamma_s^2 \lambda_q \lambda_s^2 \tilde{N}_{\Lambda}^{\Xi^*} + \gamma_s^3 \lambda_s^3 \tilde{N}_{\Lambda}^{\Omega^*}}. \quad (50)$$

$\tilde{N}_{\Lambda}^{Y^*}$ contains also (in fact as its most important contribution) the electromagnetic decay $\Sigma^0 \rightarrow \Lambda + \gamma$, and $\tilde{N}_{\Lambda}^{\Omega^*}$ includes the weak decay $\Omega \rightarrow YK$ (since Ω 's have not been reconstructed so far by WA85). If the right hand sides are evaluated using Eqs. (39, 40, 46) with $m_{\perp}^{\text{cut}} = 1.72$ GeV, for the left hand sides the experimental values (24, 25, 33) can be inserted, and Eqs. (48, 49, 50) can be solved for γ_s , λ_s , and λ_q . Note that we do not distinguish here between λ_u and λ_d since this would require the calculation of a separate decay cascade for each member of an isospin multiplet. The smallness of $\delta\mu$ in (27) justifies this approximation.

The results of our analysis are given in Tables 1 and 2 and Figures 3 and 4. Comparing the results for the thermal parameters in Table 1 with Eqs. (26, 28, 35) which contained only an estimate of the radiative Σ^0 decay but no contributions from higher lying resonances, we can draw the following conclusions:

1. The extraction of λ_q and λ_s according to Eqs. (20, 21) is only very weakly affected by resonance decays and by the origin of the slope of the m_{\perp} -spectrum (thermal or flow). (The absolute value of the associated chemical potentials does, of course, depend on the choice of the freeze-out temperature.) The reason is that in Eqs. (48) and (49) in each case the first term in the sums occurring in the numerator and denominator completely dominates. (For Ξ^- 's the effects from Ω -decays are small, and for Λ 's the strong Σ^0 contribution overwhelms the effect from Ξ^* decays.) Taking the results for the ‘‘thermal’’ scenario from Table 1 and evaluating with them the $\overline{\Xi^-}/\Xi^-$, $\overline{\Lambda}/\Lambda$, and Ξ^-/Λ ratios excluding the contributions from higher resonances changes them to 0.383, 0.121, and 0.262, respectively (instead of the input values 0.39, 0.13, and 0.20, respectively). Leaving out also the $\Sigma^0 \rightarrow \Lambda\gamma$ contribution changes only the Ξ^-/Λ ratio which now becomes 0.430. Obviously this ratio is the one which is most strongly affected by the resonance decays.
2. Since the Ξ^-/Λ ratio is the crucial ingredient for the determination of the strangeness saturation factor γ_s , the effects from resonance decays and flow can be clearly seen in this number. From Eq. (34) we had extracted $\gamma_s = 0.7$; improving the rough factor 2 estimate for the Σ^0 contribution by its correct thermal weight at $T = 210$ MeV would have lowered γ_s to 0.57. The decay of higher-lying resonances raises the value of γ_s up to 0.76 at $T = 210$ MeV. If due the presence of flow the m_{\perp} -slope does not give the true

	(a) pure “thermal” $T = 210 \text{ MeV}, \beta_f = 0$	(b) “thermal & flow” $T = 150 \text{ MeV}, \beta_f = 0.32$
λ_s μ_s/T $\mu_s \text{ (MeV)}$	0.973 −0.027 −5.7	0.972 −0.028 −4.2
λ_q μ_q/T $\mu_q \text{ (MeV)}$	1.718 0.54 113.6	1.710 0.54 80.5
γ_s	0.756	0.902

Table 1: Thermal fireball parameters extracted from the WA85 data [26] on strange baryon and anti-baryon production, for two different interpretations of the measured m_\perp -slope. Resonance decays were included. For details see text.

$N_i/N_j _{m_\perp \geq m_\perp^{\text{cut}}}$	(a) “thermal” $m_\perp^{\text{cut}} = 1.72 \text{ GeV}$	(a) “thermal” $m_\perp^{\text{cut}} = 1.2 \text{ GeV}$	(b) “flow” $m_\perp^{\text{cut}} = 1.72 \text{ GeV}$	(a) “flow” $m_\perp^{\text{cut}} = 1.2 \text{ GeV}$
$\bar{\Xi}^-/\Xi^-$	0.390*	—	0.390*	—
$\bar{\Lambda}/\Lambda$	0.130*	0.135	0.130*	0.133
Ξ^-/Λ	0.200*	—	0.200*	—
$\bar{\Xi}^-/\bar{\Lambda}$	0.600*	—	0.600*	—
Λ/p	0.625	0.617	0.888	0.867
$\bar{\Lambda}/\bar{p}$	2.044	2.084	2.833	2.802
Ω^-/Ξ^-	0.498	—	0.311	—
$\bar{\Omega}^-/\bar{\Xi}^-$	1.502	—	0.944	—
\bar{p}/p	0.040	0.040	0.041	0.041
K_s^0/Λ	0.086	0.077	0.138	0.152
K_s^0/p	0.054	0.048	0.123	0.132

Table 2: Input values (*) and predicted particle ratios for the WA85 experiment. The parameters for the “thermal” and “flow” scenarios are as in Table 1.

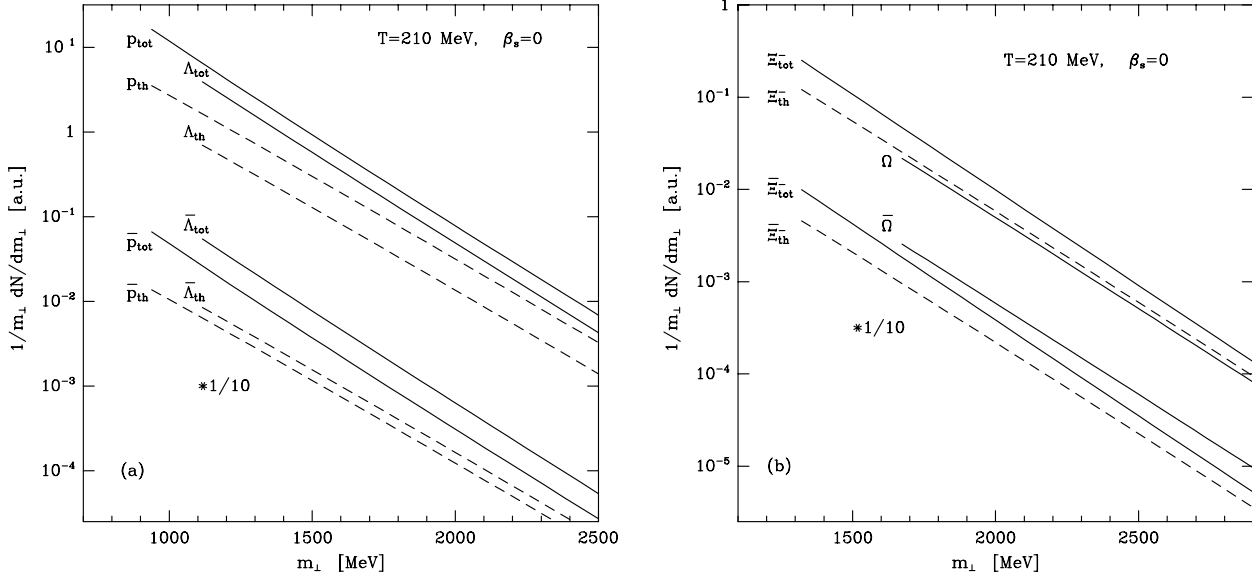


Figure 3: m_{\perp} -spectra of various baryons and anti-baryons for the “thermal” scenario (a,b) and for the “flow” scenario (c,d). The overall normalization of the spectra is arbitrary, their relative normalization is according to the fugacities from Table 1. Dashed lines indicate direct thermal production, solid lines give total yields including the contributions from resonance decays. For parameters and details see Table 1 and text.

temperature, the estimate for γ_s goes up even higher: for $T = 150$ MeV, $\beta_{\perp} = 0.32$ (*i.e.* values which are consistent with the kinetic freeze-out criterion developed in [9]) we find $\gamma_s = 0.9$, *c.f.* Table 1, corresponding to nearly complete saturation of the strange phase space!

3. The conclusion that the WA85 data on strange baryon and anti-baryon production in 200 GeV A–S collisions seem to indicate a vanishing strange quark chemical potential is extremely stable with respect to resonance decay contributions and the possibility of a flow component in the spectra. It will serve as the cornerstone of the following studies in section 4.

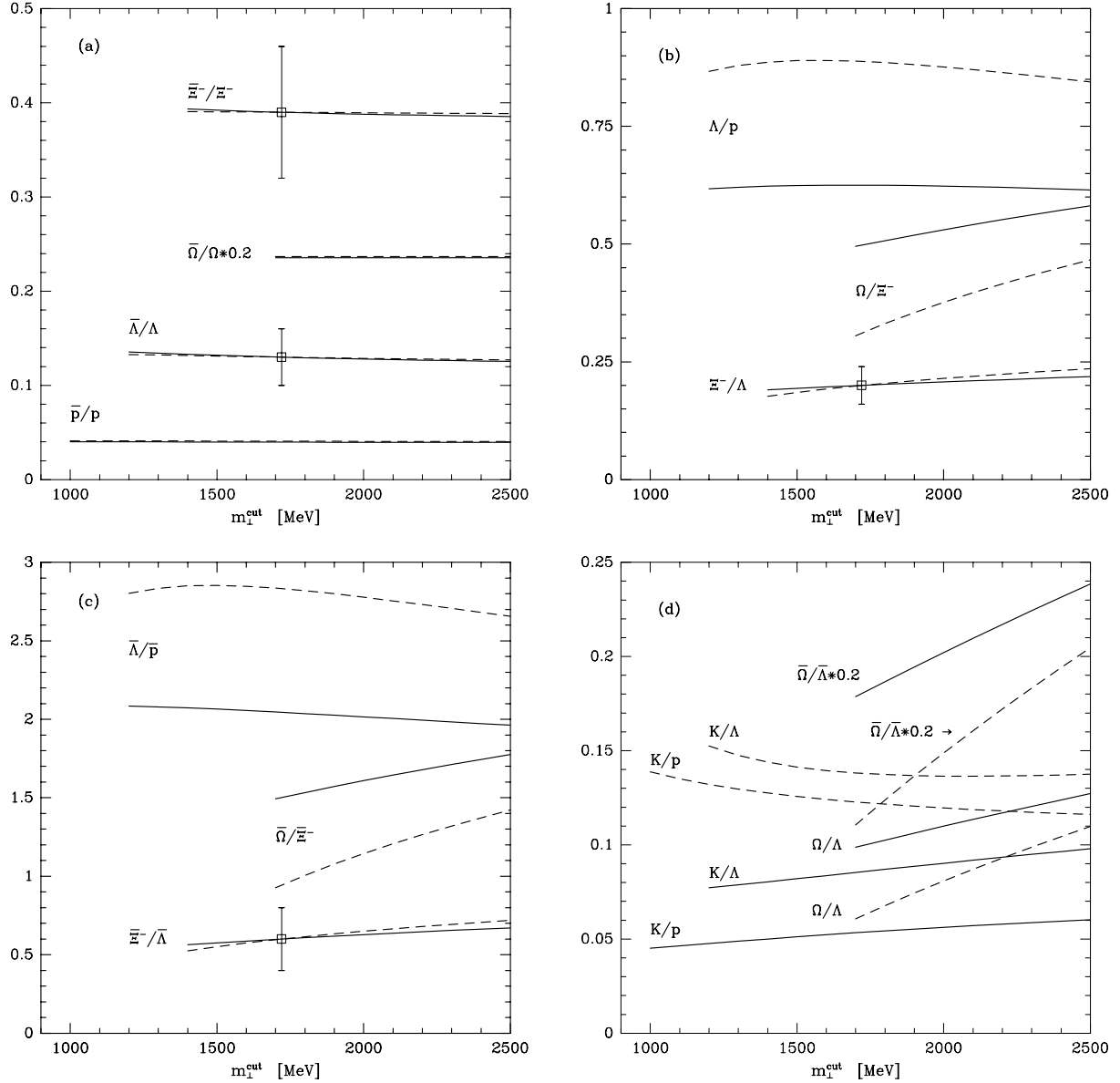


Figure 4: Various m_{\perp} -integrated particle ratios as a function of the low- m_{\perp}^{cut} . Solid lines are for the “thermal” scenario, dashed lines are for the “flow” scenario, with parameters as given in Table 1.

3.6 Particle ratios

It is clear that the extraction of three thermodynamic parameters (λ_q , λ_s , and γ_s) from three independent particle ratios cannot be considered a very convincing test of the thermal picture, in particular since the extracted values depend on the choice of the temperature whose independent derivation from the shape of the m_{\perp} -spectrum is not quite unique (unless one accepts the theoretical consistency arguments of Ref. [9] which prefer the lower temperature of around 150 MeV). It is therefore mandatory that the picture receives further experimental tests in the form of other independent particle ratios.

In Table 2 and Figure 4 we have therefore included predictions for several additional particle ratios, in particular involving $\Omega, \bar{\Omega}$ and p, \bar{p} which are expected to become soon available from the WA94 collaboration [30] in a kinematic region compatible with the WA85 results. Our calculations explore the consequences of both the “thermal” and “flow” scenarios above, and anticipate also a possible improvement of the experimental acceptance towards lower transverse momenta, by calculating in Table 2 some of the ratios also with an m_{\perp} cut of only 1.2 GeV, or plotting them (in Fig. 4) as a function of this cut.

Comparing m_{\perp} -integrated particle ratios with different m_{\perp} cuts gives an idea of the effects coming from the somewhat different slopes of thermally emitted particles and resonance decay products. From Fig. 4 we see that these effects are generally small for ratios involving only baryons: due to their heavy mass, the slope difference of parent and daughter particles in resonance decays is small [17, 9], resulting in a slight steepening of the spectra at low and intermediate m_{\perp} . For kaons, on the other hand, the decay contributions are considerably steeper than the thermal one, leading to an appreciable upward curvature of the spectrum at low m_{\perp} , while flattening out to the asymptotic apparent temperature for $m_{\perp} > 1\text{--}1.5$ GeV, where the thermal component dominates. In consequence, as seen in Fig. 4, the K/Λ and K/p ratios are proportionally more sensitive to the m_{\perp} cut.

It should be kept in mind that the large Ω/Ξ^{-} and (in particular) $\bar{\Omega}/\bar{\Xi}^{-}$ ratios are partly due to the additional spin degeneracy of the spin-3/2 Ω baryon. The apparent strong m_{\perp}^{cut} -dependence of all ratios involving Ω or $\bar{\Omega}$ baryons (especially in the flow scenario) should be taken with some caution: it results mostly from the absence of resonance decay contributions to the Ω spectrum in our calculation and might be modified if (so far unknown) Ω^* resonances existed and should be included.

When comparing different ratios involving Λ 's (*e.g.* in order to estimate the systematic of these ratios with increasing strangeness), one should always keep in mind the considerable Σ^0 contribution which, at $T = 210$ MeV, effectively changes the degeneracy factor associated with the Λ by about a factor 1.6. Once this is corrected for, *i.e.* the Σ^0 contribution is accounted for, one finds the inequalities

$$\gamma_s^2 > \frac{\Lambda\bar{\Lambda}}{p\bar{p}} > \frac{\Xi^{-}\bar{\Xi}^{-}}{\Lambda\bar{\Lambda}} > \frac{1}{4} \frac{\Omega\bar{\Omega}}{\Xi^{-}\bar{\Xi}^{-}}. \quad (51)$$

Paradoxically, Eq. (51) suggests an increasing importance of resonance decay corrections with increasing strangeness content, as compared to the estimate, Eq. (32). This is due to the fact that the stranger baryons are also heavier and thus receive less resonance contributions (because the corresponding excited states are strongly suppressed by the mass term in the Boltzmann factor) than the lighter ones (whose resonances are easier to excite). In part this tendency may be somewhat exaggerated by our cut in the resonance spectrum at about 2 GeV; taking into account even higher resonances (although it is not clear whether can indeed be excited with statistical probabilities in nuclear collisions) might modify in particular the Ω/Ξ^{-} ratios.

We regard the ratios³ predicted in Table 2 and Fig. 4 as a qualitative test of the idea

³Ratios involving protons should be taken with a grain of salt since it may not be easy experimentally to remove the contamination by cold projectile and target spectator protons. Similarly, those ratios which involve kaons may come out differently than predicted here because, as we argue in section 5, the assumption of chemical equilibrium may break down for kaons if they are created by hadronization of a QGP.

that the emitter is a fireball which is in thermodynamic equilibrium with the given thermodynamic parameters. However, even if this test is eventually passed, the fact that we can successfully describe all observed particle ratios in this way does not yet tell us immediately the nature of the emitting source (HG or QGP). That information resides in supplementary information concerning the global properties of the source and their *relationship* to the extracted thermodynamic parameters, as well as in the systematic behavior of these parameters under varying experimental conditions (collision energy, projectile and target size, collision centrality etc.). These important issues will be discussed in more detail in the following sections 4 and 5.

3.6.1 Relation between strange baryon ratios from the constrained fireball

Since thermal particle ratios are functions of only μ_B and μ_s , the accidental vanishing of μ_s at a temperature $T \simeq 200\text{--}220$ MeV due to the constraint to strangeness neutrality removes the opportunity to simply distinguish the two phases — a HG phase of strongly interacting matter, at this level of discussion, is *indistinguishable* from QGP as long as a measurement of the relative multiplicities of strange particles is considered at one, and only one collision energy. Even in this case many theoretical questions arise, such as why is $\mu_s = 0$ or why is γ_s near to unity? However, as Figs. 2a, 2b, 2c clearly show, this will not remain a problem at higher or lower temperature. To make this point more quantitative, we now study strange baryon ratios arising at different temperatures from thermal fireballs *constrained* to a (nearly) vanishing strangeness.

In Fig. 5 we show, for the case of exactly vanishing strangeness and for various temperatures, the resulting relation between R_{Ξ} and with R_{Λ} . In addition to the HG results for temperatures $T = 200$ MeV (solid line), $T = 150$ MeV (dashed line) and $T = 300$ MeV (dotted line) we show the case $\mu_s = 0$ corresponding to a QGP source hadronizing rapidly by quark recombination (dashed-dotted line). The cross corresponds to the result reported by the WA85 experiment [26]. As can be seen, the $\mu_s = 0$ curve nearly coincides with the $T = 210$ MeV curve, as noted before [6, 7], but fireballs decoupling at significantly lower or higher temperatures (as expected at lower and higher collision energies, respectively) would lead to significantly different particle ratios if the thermal model is correct.

3.6.2 High- m_{\perp} kaon abundances

In addition to the baryon ratios we can also consider the ratio of kaons to hyperons, again at fixed m_{\perp} . Because of the experimental procedures used, which rely on the observation of the disintegration of neutral strange particles into two charged decay products, a comparison of the K_s^0 with the Λ (which includes the Λ 's from the electromagnetic decay of Σ^0 's) is the most useful next step. We therefore introduce:

$$R_K \equiv \frac{K_s^0}{\Lambda + \Sigma^0} = \frac{1}{8} \frac{\lambda_s/\lambda_d + \lambda_d/\lambda_s}{\lambda_s \lambda_u \lambda_d}. \quad (52)$$

where the second identity is again, of course, only valid if resonance decay contributions can be neglected. For the rather light kaons there exist, however, many different possibilities for secondary production through resonance decays, which limits somewhat the practical

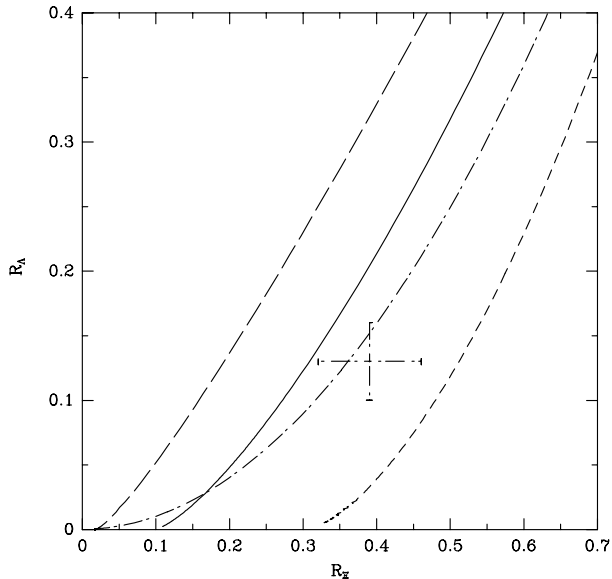


Figure 5: R_Λ versus R_Ξ . The long-dashed line corresponds to $T = 150$ MeV, the solid line to $T = 200$ MeV, and the dashed line to $T = 300$ MeV in the HG. The dashed-dotted line corresponds to QGP ($\mu_s \equiv 0$).

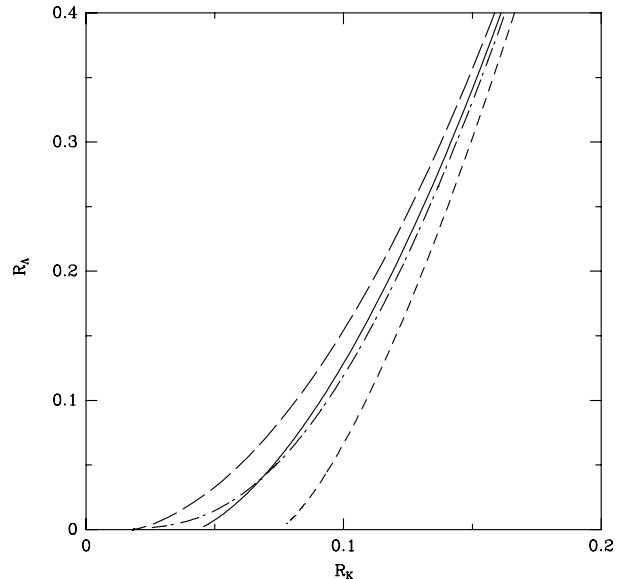


Figure 6: R_Λ versus R_K with the same conventions as in Fig. 5.

usefulness of this ratio. For example, if we use the thermodynamic parameters extracted in subsection 3.4 from the WA85 data, we obtain for the “thermal” interpretation of the m_\perp -slope ($T = 210$ MeV, no flow, $m_\perp = 1.72$ GeV) a value $R_K = 0.086$, if all resonance contributions are included, while the ground state contributions alone according to Eq. (52) would give $R_K = 0.102$ ($R_K = 0.125$ if the Λ - Σ^0 mass difference is taken into account). Since the size of these corrections depends on the fireball temperature and the m_\perp -cut, a full quantitative study does presently not appear practical.

Given these uncertainties, and in order to demonstrate the insensitivity of the K/Λ -ratio to the nature of the fireball, we show in Fig. 6 (as a matter of principle) the uncorrected ratio R_K as a function of the uncorrected ratio R_Λ : as the figure clearly shows, this observable is rather insensitive to both the temperature of the source and to its intrinsic structure ($\mu_s = 0$ or $\mu_s \neq 0$). The lines are as in Fig. 5, and we note again the near coincidence of the $T = 200$ MeV HG result with the QGP result. But even as T is changed to 150 or 300 MeV, the variation of R_Λ at fixed R_K stays well within the present experimental error bars and will thus not permit to identify the properties of the source.

4 Total particle multiplicity and entropy

We now return to discuss in detail a very important observation which is related to the particle multiplicity and charge flow associated with strange baryon production [10, 6]. Even though no data are yet available on multiplicity densities in coincidence with strange particle production, the properties of the HG and QGP fireballs with regard to their entropy content

are so drastically different that we can draw at least qualitative conclusions by comparing multiplicity data from S–Pb collisions with S–W strangeness production, despite the fact that the two targets (^{207}Pb and ^{184}W) differ slightly in mass.

QGP and HG states are easily distinguishable in the regime of values μ_B , T , γ_s of interest here. The entropy per baryon in the HG is $\mathcal{S}^{\text{HG}}/\mathcal{B} = 21.5 \pm 1.5$. Consequently, the pion multiplicity which can be expected from such a HG fireball is at best $dN/dy = 4 \pm 0.5$. This is less than half of the QGP based expectation, which we can easily estimate by considering the perturbative QGP equation of state: Up to corrections of order $(\mu_B/\pi T)^2 \sim 0.03$, the leading term of the specific entropy from light quarks and gluons is:

$$\begin{aligned} \frac{\mathcal{S}^{\text{QGP}}}{\mathcal{B}} &= \frac{3\pi^2}{2} \left(\frac{T}{\mu_q} \right) \left[\frac{14(1 - 50\alpha_s/21\pi)}{15(1 - 2\alpha_s/\pi)} + \frac{32(1 - 15\alpha_s/4\pi)}{45(1 - 2\alpha_s/\pi)} \right] \\ &= 17 (T/\mu_q) \quad \text{for } \alpha_s = 0.6 \quad . \end{aligned} \quad (53)$$

Adding to this the considerable entropy content of the strange quarks (neglecting for technical reasons the α_s -corrections in this case), we find for the QGP a specific entropy of about 45 units at the same value of T/μ_q . Poor knowledge of the value of α_s and the strange quark mass in the QGP phase make this estimate uncertain by about $\pm 15\%$. Still, the difference to the HG result is considerable in terms of experimental sensitivity. Checking the theoretical sensitivity we note that the point at which the entropy of HG and QGP coincide *and* strangeness vanishes *and* $\lambda_s \simeq 1$ is at $T \simeq 135$ MeV, $\mu_B \simeq 950$ MeV, quite different from the region of interest here. We therefore consider now an observable which is capable to distinguish between the HG and QGP via their entropy content.

4.1 EMU05 data

Total charged particle multiplicities (excluding target/projectile fragments) *above* 600 in the central region have been observed by EMU05 [11] in 200 GeV A S–Pb collisions, corresponding possibly to a total particle multiplicity of as large as 1000. We believe that such large multiplicities are implied by a QGP scenario for the central fireball, while being hardly compatible with the corresponding HG interpretation. The data of the EMU05 collaboration [11] were obtained with a high multiplicity “trigger” which makes them useful in comparison with the WA85 results which are also triggered on high multiplicity. Some of these charged multiplicity data from emulsions are shown as a function of rapidity in Fig. 7. We depict the quantity D_Q , the difference in the number of positively and negatively charged particles normalized by their sum [11]:

$$D_Q \equiv \frac{N^+ - N^-}{N^+ + N^-} \quad (54)$$

The data points correspond to 15 fully scanned “central” events of 200 GeV A S–Pb interactions, with the trigger requirement being a total charged multiplicity > 300 . Reaction spectators (target fragments) are not observed in this experiment. At central rapidity a value of 0.08–0.09 is found for D_Q . We note the rise of D_Q in the projectile and target pseudorapidity regions, indicating a more rapid decrease of the particle multiplicity (mostly pions) than of the positive particle excess (protons). Obviously this feature proves the partial transparency at CERN energies of the Pb nucleus to the incoming sulphur projectile; it will

be quite interesting to see if this feature persists for heavier projectiles and in particular how the shape is in Pb–Pb collisions.

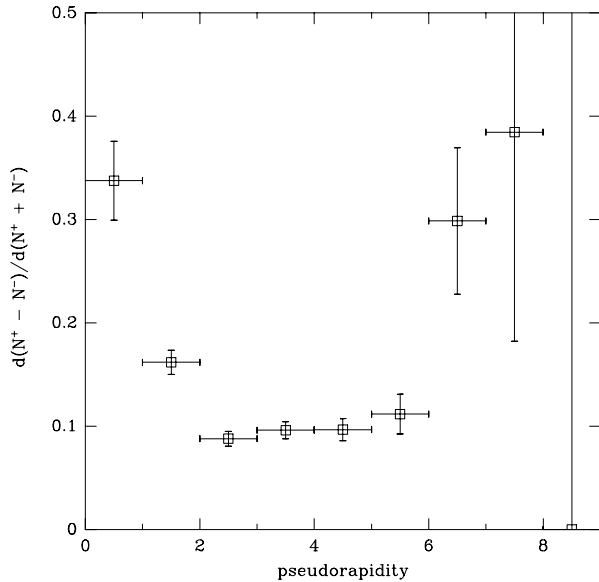


Figure 7: Emulsion data for charged particle multiplicity as function of pseudo-rapidity: the difference of positively and negatively charged particles normalized by the sum of both polarities. (Courtesy of EMU05 collaboration, Y. Takahashi et al. [11]).

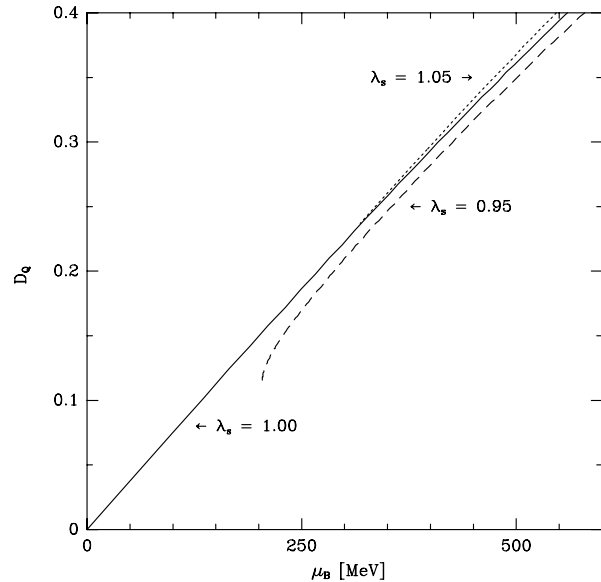
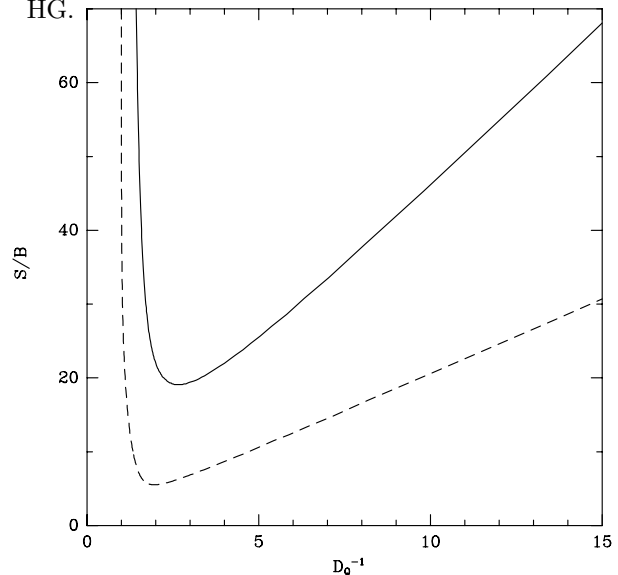


Figure 8: D_Q as a function of μ_B for fixed $\lambda_s = 1 \pm 0.05$ and conserved zero strangeness in HG.

Figure 9: Entropy per baryon \mathcal{S}/\mathcal{B} as a function of D_Q^{-1} for fixed $\lambda_s = 1$ and conserved zero strangeness. The lower, dashed curve does not take into account the strange hadrons.



In our theoretical work we address primarily the central region, in which the smallest values of D_Q indicate the highest multiplicity production.

4.2 Significance of D_Q

The numerical evaluation of D_Q in a HG at $\lambda_s = 1 \pm 0.05$, where we fix the temperature for each μ_B such that strangeness is conserved, is shown in Fig. 8. We see that approximately

$$D_Q \approx \frac{\mu_B}{1.3 \text{ GeV}} \quad \text{for} \quad \mu_B < 0.6 \text{ GeV}. \quad (55)$$

This HG result is extremely simple, considering the complexity of the calculation. We thus see that in the only permissible HG scenario for the strangeness source which (according

to Eq. (29)) *has to have* $\mu_B \sim 0.34$ GeV, Eq. (55) would predict a value of $D_Q \sim 0.26$; this is incompatible with the EMU05 results, see Fig. 7, where the central value is $D_Q(y = 2.5 \pm 0.5) = 0.088 \pm 0.007$. At this value of D_Q the HG phase would have $\mu_B = 115$ MeV, rather than the 340 MeV we have extracted from the strange baryon data. Despite the fact that both measurements use different targets we believe that we can draw the conclusion that a HG fireball is incompatible with the combined EMU05 and WA85 data.

Physically the variable D_Q represents essentially the inverse of the specific entropy. The measured very small value of D_Q thus implies a very large value for \mathcal{S}/\mathcal{B} . In Fig. 9 we show the specific entropy as a function of D_Q^{-1} for a zero-strangeness hadron gas at $\lambda_s = 1$. We see the very strong direct correlation between these two quantities. We supplement this observation in Figs. 10a, 10b, and 10c by also showing \mathcal{S}/\mathcal{B} as a function of D_Q^{-1} at fixed $T = 150, 200, 300$ MeV, varying $\epsilon = 0, \pm 0.1$. We observe that, within the range of these parameters, the small observed value of D_Q always requires a rather large specific entropy $\mathcal{S}/\mathcal{B} = 50 \pm 4$. Thus D_Q^{-1} effectively measures the entropy per baryon, independent of the specific thermal conditions of the source.

Please note that in this connection it is essential to correctly account for the strange particles. To illustrate this point and to understand the value of D_Q we show in Fig. 11 the product $D_Q \cdot (\mathcal{S}/\mathcal{B})$ as a function of μ_B for fixed $\lambda_s = 1 \pm 0.05$, where akin to Fig. 9, the lower set of curves was obtained without strange particles. We see that strange particles have considerable impact on the result.

Both the limiting value and near constancy of the result obtained without strange particles can be easily understood since in this case $D_Q \cdot (\mathcal{S}/\mathcal{B})$ is effectively the entropy per pion. To see this note that in absence of strange particles we have (neglecting the small $u-d$ asymmetry and assuming pion symmetry $N_{\pi^+} = N_{\pi^-} = N_{\pi^0} = N_{\pi}/3$):

$$D_Q \rightarrow 0.75 \frac{\mathcal{B}}{N_{\pi}} \frac{1}{1 + 1.5 \sum_i N_i/N_{\pi}} \quad (56)$$

where the last term in the denominator involves the sum over all initial charged particles other than pions, in particular heavy mesons, protons and anti-protons, etc. Considering the product of D_Q with \mathcal{S}/\mathcal{B} , the baryon content cancels and the result is effectively entropy per pion renormalized (as it turns out numerically with a factor 2) by the degeneracy factors and resonance contributions. This also explains why the product is rather constant as μ_B (and along with it T) changes: there is a slow increase in the entropy per pion with increasing μ_B since the resulting decrease in T enhances the relative importance of the heavier baryon resonances with the associated larger entropy per particle.

The question arises whether the QGP fireball model would be in better agreement with the combined WA85 and EMU05 data, or if the disagreement of the HG picture with the data is rather an indication for the failure of the fireball model in general. In order to be able to answer this question in detail we need in principle to have a sophisticated model for the hadronization of a QGP. However, as long the final state is one with thermal momentum distributions, the relationship between D_Q and \mathcal{S}/\mathcal{B} is likely to be similar to that of Fig. 9 even if the observed hadrons result from a hadronizing QGP. The reason is that the product $D_Q \cdot (\mathcal{S}/\mathcal{B})$ (in other words, the entropy per pion) will not deviate drastically from its equilibrium hadron gas value even in a state which is considerably out of chemical equilibrium. Noting that there is little entropy production in the QGP hadronization process [33] we can

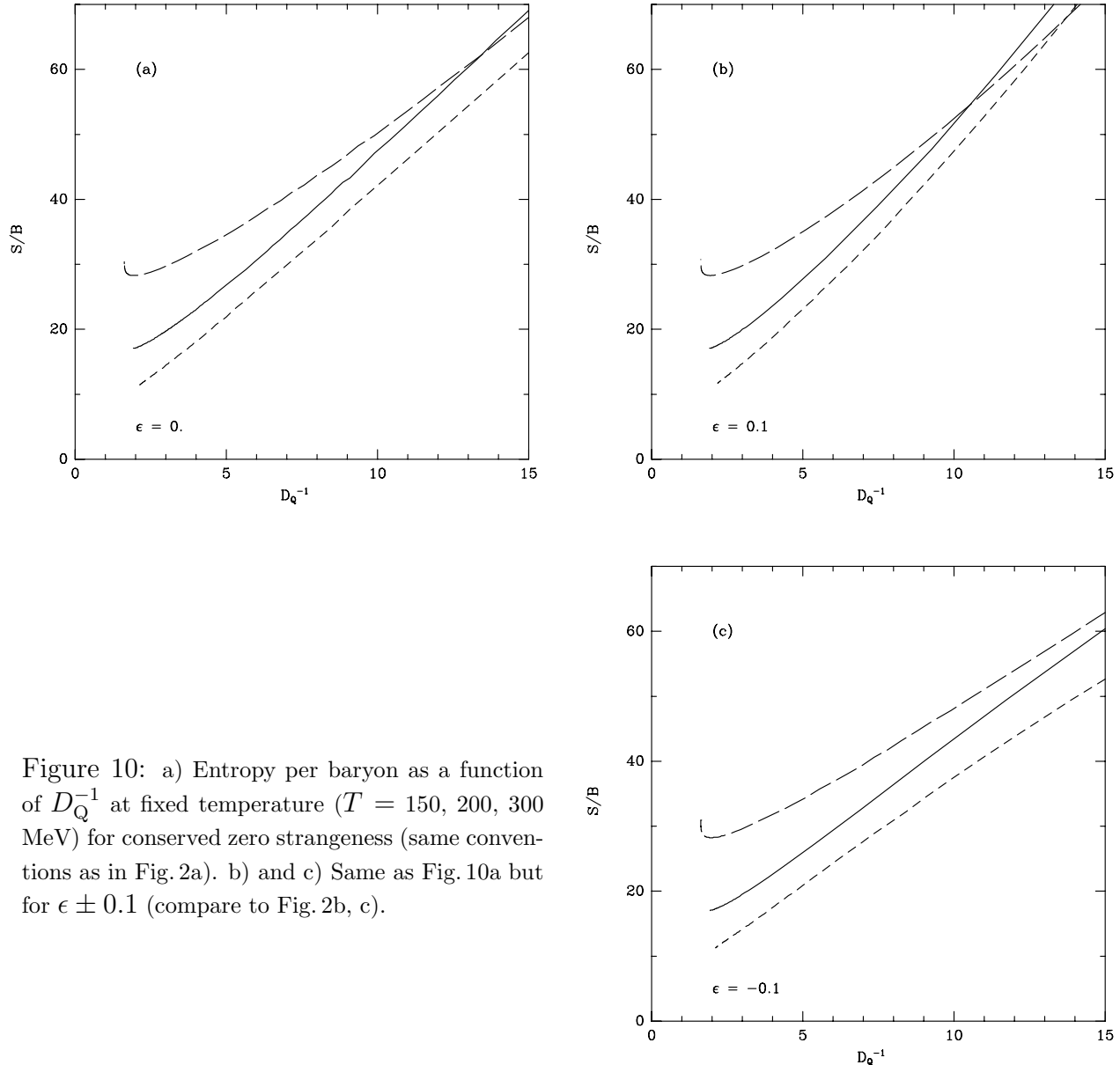


Figure 10: a) Entropy per baryon as a function of D_Q^{-1} at fixed temperature ($T = 150, 200, 300$ MeV) for conserved zero strangeness (same conventions as in Fig. 2a). b) and c) Same as Fig. 10a but for $\epsilon \pm 0.1$ (compare to Fig. 2b, c).

thus subsume that after hadronization the result would be a point close to the curve shown in Fig. 9. We see that the value $D_Q \simeq 0.09$ implies $S/B \sim 50$, which is indeed of the order required by a hadronizing QGP with the thermal parameters extracted in section 3. We note that entropy per baryon is a dimensionless function of the dimensionless quantity T/μ_B and hence different QGP scenarios with the same T/μ_B all have the same value of the entropy per baryon.

As the result of this study we conclude that the charge flow ratio with the charged particle multiplicity is an excellent experimental measure of the entropy per baryon in the source, and that the current results are suggestive of a much more entropy-rich emitter at central rapidity than can be expected in hadronic gas models.

4.3 NA35 data

Even though the use of thermal model is less convincing for the small collision system S-S, we will shortly consider the results obtained by the NA35 collaboration [34, 35] in S-S interactions at 200 GeV A. In this case we can base our discussion on the reported charged particle rapidity densities [35] and the measured $\bar{\Lambda}/\Lambda$ ratio [34]. S-S interactions show at central rapidity visibly less baryon number stopping than S-W collisions; from the data on $d(N^+ - N^-)/dy$ and dN^-/dy in [35] we read off a central rapidity value of $D_Q^{S+S}(y=3) = 0.065$. The raw $\bar{\Lambda}/\Lambda$ ratio (uncorrected for Ξ -decays) is strongly peaked at central rapidity and rises there to a value $\bar{\Lambda}/\Lambda = 0.34$ (with error bars of order 50%) [34]. The observed transverse mass spectra can again be interpreted in terms of a thermal, longitudinally expanding central fireball with $T \simeq 200$ – 220 MeV [17] or, including a transverse flow component, by $T \simeq 150$ MeV combined with a flow velocity $\beta_f \simeq 0.3$ [9].

Following Eq. (21), the asymmetric $\bar{\Lambda}/\Lambda$ ratio implies a non-zero combination of chemical potentials, $\mu_B + (3/2)\mu_s \simeq (0.8 \pm 0.4)T$. We note that the experimental ratio decreases when averaged over a larger rapidity interval, implying even larger chemical potentials. If $T \simeq 210$ MeV, both the HG and QGP model imply $\mu_s \simeq 0$ for strangeness neutral systems, and we thus obtain $\mu_B \simeq 170 \pm 85$ MeV. For the “flow” scenario with $T = 150$ MeV, strangeness conservation in a HG allows the above relation to be satisfied with $\mu_s \simeq 17$ MeV at $\mu_B \simeq 95$ MeV, again with rather large experimental errors.

For the “thermal” case we can use Fig. 8 to translate μ_B into D_Q ; with $\mu_B = 170 \pm 85$ MeV we obtain $D_Q \simeq 0.13 \pm 0.06$. Although the central value of D_Q extracted in this way is twice the measured value for this ratio, due to the large experimental uncertainty of the $\bar{\Lambda}/\Lambda$ ratio the two numbers still agree within one standard deviation. We note that a HG with $D_Q = 0.13$ possesses a specific entropy $\mathcal{S}/\mathcal{B} = 35$, while $D_Q = 0.065$ requires $\mathcal{S}/\mathcal{B} = 65$ – 75 . For the “flow” scenario, on the other hand, we compute with the conventional HG-EoS (with $\mu_B = 95$ MeV, $\mu_s = 17$ MeV) a value $D_Q \simeq 0.05$, consistent with the measured value 0.065.

As this discussion demonstrates, the current NA35 strange particle data are neither precise enough nor do they provide sufficiently complete information to allow for a similar analysis as done for the WA85 data above. In particular the lack of data on Ξ^- and $\bar{\Xi}^-$ production in S-S collisions prevents us from determining the values of γ_s and μ_s . In the absence of such information, the validity of a HG description for the NA35 S-S data can at the present moment not be excluded.

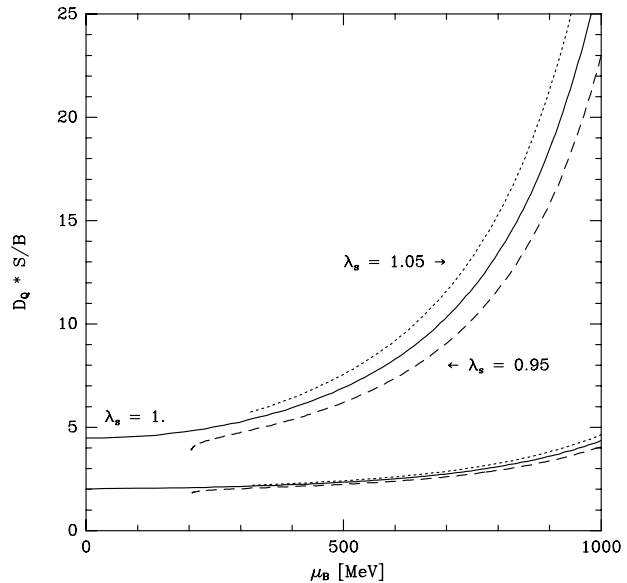


Figure 11: The product $D_Q \cdot (\mathcal{S}/\mathcal{B})$ as function of μ_B for fixed $\lambda_s = 1 \pm 0.05$ and zero strangeness (compare to Fig. 8). The lower set of curves was obtained without including strange particles.

5 Implications for the fireball evolution dynamics

So far we have extracted, with the help of thermodynamical concepts, from various sets of nuclear collision data the characteristic statistical properties of the source of the emitted particles. In the following we will comment on what our findings imply for the possible formation of a quark-gluon plasma, for its evolution and ultimately its dissociation into the final state hadrons.

We have seen that a HG interpretation of the WA85 data on strange baryon production is not consistent with the large multiplicity densities observed by EMU05 which indicate a much larger specific entropy than implied by the HG picture. In this context we have discussed both a “purely thermal” interpretation of the data (which identifies the slope of the transverse mass spectra directly as the fireball temperature) and a “flow scenario”, where part of the observed slope is due to a blueshift factor caused by transverse collective expansion of the fireball. Independent of which version of the HG picture we used, we found from the WA85 data a surprisingly large degree of strangeness saturation γ_s , ranging from 75% in the purely “purely thermal” interpretation to 90% in the “flow scenario”. These are hard to understand in a HG scenario, because the time scale for strangeness producing processes is usually believed to be much too slow to achieve that kind of saturation during the lifetime of the collision, unless a QGP is formed.

Within the HG picture, the dynamical aspects connected with the flow seem to be required for consistency with the freeze-out kinetics [9]. For this reason the “flow scenario” has been highly favored before. However, we have shown here that within the HG picture the value $\mu_s = 0$ constrains the liberty to interpret the slope of the transverse mass spectra in terms of a temperature which is blueshifted by flow. The observed values $\mu_s = 0$ and $\mu_B/T = 1.63$ are inconsistent with strangeness neutrality of the observed system of hadrons at the rather low value of $T \simeq 150$ MeV resulting from the “flow” picture. To recover consistency with the strangeness neutrality of the fireball under these conditions, the HG equation of state would have to be very different from the conventional Hagedorn resonance gas which we employed here. While such a major modification of the physics of the hadron phase cannot at present be completely excluded, it would invalidate a large body of successful phenomenological work based on the conventional HG picture. Thus, if the experimental result $\mu_s = 0$ should be confirmed via other particle ratios, in our opinion it practically eliminates within the framework of a conventional HG-EoS the flow interpretation of the spectra as a viable alternative to the purely “thermal” interpretation.

We therefore conclude that within a HG picture the interpretation of the m_{\perp} -slope of $\simeq 210$ MeV as the true temperature of the fireball appears to be the only possibility consistent with the constraint of (approximate) strangeness neutrality. This excludes the possibility of transverse flow, however, and thus causes consistency problems for the freeze-out process. In addition, it does not lead to the observed value of D_Q . Therefore a HG interpretation of the data appears to be excluded.

If one tries instead to interpret the observations in terms of QGP formation, one faces the problem to understand how the hadronization process can lead to a final state with the observed values for the thermodynamic parameters. We have seen that the conditions of strangeness neutrality and of a fixed up-down asymmetry in general lead, at the same temperature, to different values for the chemical potentials μ_u, μ_d, μ_s in the two phases. While

a vanishing value of μ_s is a natural consequence of strangeness neutrality in the QGP, it is not at all natural in the hadron gas, where $\mu_s = 0$ solves the strangeness neutrality condition only for very specific pairs of T and μ_B , and thus in general it is not a value expected to arise in an interpretation of the experiments involving HG fireballs. On the other hand, while the values of the chemical potentials assumed in a hadron gas can be directly determined from the measured abundance ratios between the various hadronic species emitted by the gas, this is not automatically true for the QGP chemical potentials. How μ_u , μ_d , and μ_s inside the QGP are related to the abundance ratios of the finally observed hadrons depends on the dynamical and kinetic details of the hadronization process.

To illustrate this problem, let us consider the limiting case of a very long-lived and slowly hadronizing quark-gluon plasma, where hadronization proceeds through a mixed phase providing intimate contact between the two sub-phases. In this case chemical equilibrium not only within the hadronic sub-phase (with respect to processes which transform the hadrons among each other) and within the quark sub-phase (with respect to processes transforming quarks and gluons into each other), but also between the two phases (with respect to processes which create hadrons out of quarks and gluons or dissociate them again into quarks and gluons) can be maintained. As a consequence, the chemical potentials change smoothly from their values originally assumed in the QGP phase into the chemical equilibrium values of the hadron gas, and only the latter (and not the former) would be observable by studying particle ratios. In such a scenario, the value of the strange quark chemical potential μ_s extracted from a suitable combination of strange hadron abundances [3] would in general not be zero (although it started out as zero in the original QGP phase), but would be given by the solution to the strangeness balance constraint (14) in an equilibrated hadron gas.

However, as demonstrated in this paper, the strange particle yields from the WA85 collaboration [26] indeed do point to a value of $\mu_s = 0$, and in view of the naturalness of this value in the context of a QGP we are inclined to believe that this result may not be entirely accidental. Therefore we ask under which conditions $\mu_s = 0$ could have survived the QGP hadronization process after all.

One possibility to transfer the QGP values for the chemical potentials and temperature directly to the final state hadrons is to assume rapid break-up of the QGP combined with statistical quark recombination [3, 13, 31, 32]. A necessary condition for the preservation of the QGP thermodynamic parameters is that sequentially produced hadrons escape sufficiently rapidly such that there is no formation of an intermediate HG phase in which the chemical potentials and/or momentum distributions could re-equilibrate. One can view this process as the peeling of the QGP surface into the vacuum — since there is no barrier, the surface regions of the QGP fireball are peeled off in form of rapidly escaping hadrons, carrying in their abundances the information about the thermal and chemical properties of the QGP.

One problem with such a picture is that the system of radiated hadrons, described by thermal distributions with chemical potentials and temperature as given originally in the QGP phase, by definition is characterized by the same particle abundance ratios and by the same value of the specific entropy as an equilibrium HG at the same temperature. The radiation obtained from this quark recombination picture is in general neither strangeness

neutral⁴, nor does it carry away the correct amount of entropy per baryon (as fixed by the original QGP) It is well known that the entropy balance can be saved by considering the entropy contained in the gluons of the QGP, letting them materialize as hadrons via gluon fragmentation into additional quark-anti-quark pairs. In [13] the additional quarks from gluon fragmentation were hadronized according to the same laws of combinatorics as the thermal quarks from the QGP; as a result the QGP chemical potentials were not preserved, but the quark chemical potentials were modified during hadronization in the direction of their HG equilibrium values.

The minimal dynamical picture could consist of a primordial explosive production of the few high m_{\perp} strange anti-baryons, followed by equilibrium hadronization of the remaining fireball at nearly constant entropy. To test such a picture requires the simultaneous measurement of the abundances and momentum spectra of (strange and non-strange) baryons and anti-baryons and of (fully identified) pions and kaons. Only with such a complete set of data on produced hadrons can a full understanding of the evolution of the primordial dense phase (QGP?) be achieved.

Of course, our contention that the presently available data are inconsistent with a HG picture for the collision and rather point to a very entropy-rich source of particle emission, possibly a quark-gluon plasma, must appear provocative at the present stage. Our findings show that it is necessary to widen the investigation of strange anti-baryon ratios to higher *and* lower nuclear beam energies and to study simultaneously the particle multiplicity and charge flow at high and low m_{\perp} , in order to confirm the now very suggestive conclusion of QGP formation in the collisions of S ions at 200 GeV A with heavy nuclear targets at near zero impact parameter. In view of the ambiguity between the HG and QGP picture, as far as the consistency of a vanishing strange quark chemical potential with the condition of strangeness neutrality is concerned, the presently available beam energies at CERN turn out to be somewhat unfortunate, due to the observed particular value of around 210 MeV for the m_{\perp} -slope; this ambiguity could be easily resolved if $\mu_s = 0$ were still observed in cases where the m_{\perp} -slope (apparent temperature) is lower or higher. It is natural to expect such a variation in the slope parameters (combined by an inverse variation of the baryon chemical potential) once collisions at lower or higher beam energies are studied (for example with a 50 GeV A Pb-beam at the CERN SPS or with 100+100 GeV A Au-beams at RHIC). We are also looking forward with anticipation to the forthcoming Pb–Pb collisions at about 170 GeV A projectile energy, which will allow to check and extend the results of our analysis by going to the largest possible thermodynamic systems using nuclear collisions.

Acknowledgements: J.R. thanks his colleagues in Paris and Regensburg for their warm and personal hospitality. The work of U.H. and J.S. was supported by DFG, BMFT and GSI. The collaboration between U.H. and J.R. was supported by NATO Collaborative Research Grant 910991. J.R. acknowledges funding of his research by DOE, grant DE-FG02-92ER40733.

⁴We thank H. Satz for bringing this point to our attention.

References

- [1] See “Quark Matter ’91”, T. C. Awes *et al.* (eds.), *Nucl. Phys.* **A544** (1992).
- [2] J. Rafelski, *Nucl. Phys.* **A544** (1992) 279c, and references therein.
- [3] J. Rafelski, *Phys. Lett.* **B262** (1991) 333.
- [4] J. Rafelski and A. Schnabel, in: *Intersections Between Particle and Nuclear Physics*, G. M. Bunce (ed.), AIP Conference Proceedings **176**, American Institute of Physics, New York, 1988, p. 1086 (see in particular Fig. 1).
- [5] H.-C. Eggers and J. Rafelski, *Int. J. Mod. Phys.* **A6** (1991) 1067 (see in particular Fig. 8)
- [6] J. Letessier, A. Tounsi and J. Rafelski, *Phys. Lett.* **B292** (1992) 417
J. Letessier, A. Tounsi and J. Rafelski, *Strange Anti-Baryons – QGP versus HG*, Paris preprint PAR/LPTHE/92-32, to appear in the proceedings of the International High Energy Physics Conference, Dallas, TX, August 1992, American. Inst. of Physics, 1993.
- [7] J. Cleymans and H. Satz, *Thermal Hadron Production in High Energy heavy Ion Collisions*, preprint CERN-TH 6523/92 (BI-TP 92/08), *Z. Phys.* **C**, in press.
- [8] J. Rafelski, H. Rafelski and M. Danos, *Phys. Lett.* **B294** (1992) 131
- [9] K. S. Lee, U. Heinz, and E. Schnedermann, *Z. Phys.* **C48** (1990) 525;
E. Schnedermann and U. Heinz, *Phys. Rev. Lett.* **69** (1992) 2908;
E. Schnedermann, J. Sollfrank, and U. Heinz, *Fireball Spectra*, in: *Particle Production in Highly Excited Matter*, H. H. Gutbrod (ed.), Plenum, New York, in press.
- [10] J. Letessier, A. Tounsi, U. Heinz, J. Sollfrank and J. Rafelski, *Evidence for a high Entropy phase in nuclear collisions*, preprint PAR/LPTHE/92-37, submitted to *Phys. Rev. Lett.*
- [11] Y. Takahashi et al., CERN-EMU05 collaboration, private communication.
- [12] U. Heinz, P. Koch, and B. Friman, in: *Proceedings of the Large Hadron Collider Workshop*, Aachen, 1990, G. Jarlskog and D. Rein (eds.), CERN report CERN 90-10, Vol. II, p. 1079.
- [13] P. Koch, B. Müller, and J. Rafelski, *Phys. Rep.* **142** (1986) 167.
- [14] J. Rafelski, *Phys. Lett.* **B190** (1987) 167.
- [15] P. Koch, J. Rafelski and W. Greiner, *Phys. Lett.* **123B** (1983) 151.
- [16] N. K. Glendenning and J. Rafelski, *Phys. Rev.* **C31** (1985) 823.
- [17] J. Sollfrank, P. Koch, and U. Heinz, *Phys. Lett.* **B253** (1991) 256; and *Z. Phys.* **C52** (1991) 593

- [18] J. Rafelski and B. Müller, *Phys. Rev. Lett.* **48** (1982) 1066.
- [19] P. Koch and J. Rafelski, *Nucl. Phys.* **A444** (1985) 678.
- [20] R. Hagedorn, I. Montvay, and J. Rafelski, “Thermodynamics of Nuclear Matter from the Statistical Bootstrap Model”, in: *Hadronic Matter at Extreme Density*, N. Cabbibo and L. Sertorio (eds.), Plenum, New York, 1978.
- [21] M. Kataja, J. Letessier, P.V. Ruuskanen, and A. Tounsi, *Z. Phys.* **C55**, (1992) 153.
- [22] C. Greiner, P. Koch, and H. Stöcker, *Phys. Rev. Lett.* **58** (1987) 1825;
C. Greiner, D. H. Rischke, H. Stöcker, and P. Koch, *Phys. Rev.* **D38** (1988) 2797.
- [23] U. Heinz, K. S. Lee, and M. Rhoades-Brown, *Mod. Phys. Lett.* **A2** (1987) 153;
K. S. Lee, M. Rhoades-Brown, and U. Heinz, *Phys. Rev.* **C37** (1988) 1452.
- [24] K. S. Lee and U. Heinz, *The phase diagram for strange hadronic matter*, Regensburg preprint TPR-92-20, submitted to *Phys. Rev.* **D**.
- [25] J. Cleymans, *Nucl. Phys.* **A525** (1991) 205c.
- [26] S. Abatzis *et al.*, *Phys. Lett.* **B270** (1991) 123; and **B259** (1991) 508.
- [27] E. Andersen *et al.*, NA 36 Coll., *Phys. Lett* **B294** (1992) 127
- [28] L. Csernai, N.S. Amelin, E.F. Staubo and D. Strottman, Bergen University Report 1991-14, table 4, submitted to *Phys. Rev.* **C** and private communication.
- [29] T. Åkesson *et. al.*, AFS-ISR Collaboration, *Nucl. Phys.* **B246** (1984) 1.
- [30] WA94 proposal, E. Quercigh *et al.*, CERN/SPSLC 91-5 P257 (1991).
- [31] T. S. Biró and J. Zimányi, *Nucl. Phys.* **A395** (1983) 525.
- [32] J. Rafelski and M. Danos, *Phys. Lett.* **B192** (1987) 432.
- [33] B. L. Friman, G. Baym, and J.-P. Blaizot, *Phys. Lett.* **B132** (1983) 291;
H. W. Barz, B. Friman, J. Knoll, and H. Schulz, *Nucl. Phys.* **A484** (1989) 661.
- [34] J. Bartke *et al.*, NA35 Coll., *Z. Phys.* **C48**, 191 (1990).
- [35] S. Wenig, Ph.D. Thesis Frankfurt/M, GSI Report 90-23 (1990), and NA35 Coll., to be published.